Riparian Zone Estimation Tool Hydrologic Connectivity Module

Documentation and Validation of Selected Methodology

CONTRIBUTION NO. 745
FEBRUARY 2015

Prepared by the San Francisco Estuary Institute
Wetlands Focus Area

Decision Support Tool for Appropriately Sizing Riparian Buffers
Proposition 50 CALFED Watershed Protection Grant Program
Grant Agreement Number: #10-429-550
June 9, 2011 – March 31, 2015

SAN FRANCISCO ESTUARY INSTITUTE
4911 Central Avenue, Richmond, CA 94804
p: 510-746-7334 (SFEI) • www.sfei.org

Funding for this project was provided in full or in part through an agreement with the State Water Resources Control Board. The project does not necessarily reflect the views and policies of the State Water Resources Control Board, nor does mention of trade names or commercial products within any of the documentation constitute endorsement or recommendation for use.

For more information please contact:
Scott Dusterhoff, scottd@sfei.org
510-746-7350

THIS REPORT SHOULD BE CITED AS:
SFEI (2015). Riparian Zone Estimation Tool. Hydrologic Connectivity Module. Documentation and Validation of Selected Methodology. Prepared by the San Francisco Estuary Institute - Wetlands Focus Area. Funded by Proposition 50 Watershed Protection Program Grant. Agreement Number: #10-429-550. Contribution #745. Richmond, CA 94804.

Riparian Zone Estimation Tool
Hydrologic Connectivity Module
Documentation and Validation of Selected Methodology

February 24, 2015

Introduction

Background & Purpose

The loss of riparian areas throughout California has greatly impacted water quality and habitat conditions, which has resulted in a number of challenges for resource managers and the public in terms of water management and land use planning. Riparian areas, defined here as floodplain areas adjacent to streams and wetlands, provide a multitude of functions or ecologic services for their adjacent aquatic habitats including shading, bank stabilization, organic and inorganic input, filtration, ground water recharge, and downstream flood reduction. In the face of ongoing development and climate change, there is a great need for land use planners to have tools available that can help them delineate and map the desired extent of riparian functional areas in developed watersheds targeted for restoration or relatively undisturbed watersheds targeted for development.

To increase the ability to enhance and protect riparian zones, SFEI received funding from the Proposition 50 CALFED Watershed Protection program to develop a geospatial tool capable of delineating the desired extent of riparian functional areas by building upon our existing Riparian Areas Mapping Tool (RAMT). RAMT is a Geographic Information System (GIS)-based tool that estimates riparian functional area associated with vegetation-related (e.g., large woody debris input, shading, bank stabilization) and hillslope-related (e.g., coarse sediment input) riparian functions. The tool uses publicly available input data combined with representative values taken from published literature and scientific expertise to generate functional riparian widths based on existing land use, vegetation, and slope. This project seeks to expand the RAMT by developing a new module that uses local flow hydraulics to size riparian areas along higher order, lower gradient alluvial stream channels based on functions identified as important by the State Water Resources Control Board including flood attenuation, runoff reduction, and aquatic habitat and water quality improvement. The final product for this project will be a scientifically based Riparian Zone Estimation Tool (RipZET) that combines the existing two RAMT modules with the new module, called the Hydrologic Connectivity Module (HCM).

In undisturbed lower gradient alluvial channel valleys, riparian vegetation typically exists out to the inundation extent for larger floods (Ilhardt et al. 2000). As such, the HCM is being developed to assess local flooding extent as a means of determining functional riparian areas for either developed or undisturbed channel reaches. Within the HCM, reach-scale flooding is assessed as a function of discharge, topography, and boundary roughness using what is termed the "Discharge Approach." Flooding extent is determined in this approach using a modified form of Manning's equation:

$$Q = \frac{1.486(A)(R^{2/3})(S^{1/2})}{n}$$

where;
Q = flow discharge (ft^3/s),
A = flow area (ft),
R = hydraulic radius (similar to average flow depth, ft)
S = slope of the energy grade line (similar to reach-average channel bed slope, ft/ft), and
n = roughness factor.

Using this simple hydraulic equation with local channel-floodplain topography and roughness data enables calculation of flow depth and flow width (or inundation extent) for a range of flow discharge values. Combining this output with local flood frequency information allows determining flooding extents of major, geomorphically effective floods (e.g., the 10- to 50-year floods), which in turn can be used to estimate the appropriate functional riparian width for lower gradient alluvial channels (*cf*. Ilhardt et al. 2000).

Developing useful flooding extent estimates capable of sizing functional riparian widths requires high quality, high resolution data. As the HCM needs to be easy to use within the RipZET desktop tool and based in large part on readily available data, module development requires understanding how module output is affected by input data sources. For example, it is important to know the degree to which flooding extents calculated using field-based topographic data differ from flooding extents calculated using publically available but lower resolution remote spatial data (e.g., LiDAR data). Once the effects of input data source on module output are understood, it is possible to develop recommendations regarding the necessary data sources for running the HCM.

This report provides the results from a study aimed at validating the HCM approach and assessing the effects of input data source resolution on the HCM approach output. The specific research questions guiding this study were:

1. Does the HCM approach adequately predict local hydraulic conditions for a range of flood flows using intensive field data?; and
2. Do readily available alternate or remote data sources provide similar results as intensive field data?

We answer these questions here by analyzing data from several channel locations around the North Bay (Marin, Napa, and Sonoma counties). The analysis focuses on comparisons of: 1) measured hydraulic conditions and hydraulic conditions calculated using the HCM approach; and 2) calculated hydraulic conditions at individual sites using variable input data. At the conclusion of the report, we synthesize the study results into an assessment of the HCM approach efficiency and ease of use for developing a functional riparian area estimate, key considerations when using the HCM approach, overall HCM approach advantages and limitations, and recommended next steps for improving the HCM approach.

Overall Study Approach

This study began with collecting channel topographic and roughness data at eight representative North Bay channel locations, including sites from the recent RipZET Regional Curve Study (Collins and

Leventhal 2013). At each site, we surveyed cross-sections that included both the channel and floodplain. In addition, we estimated channel roughness for both the channel and floodplain at each cross-section location using a widely used protocol based on bed particle size distribution, channel morphology, and in-channel and floodplain vegetation characteristics. We then used the compiled data to develop flow stage-discharge relationships (i.e., rating curves) that can be used with local peak flood discharge estimates to determine flooding inundation extent. Rating curves developed from intensive field data and readily-available alternate data sources (e.g., LiDAR topographic data) were then compared to assess the utility of the alternate data sources.

Data collection and analysis occurred from Fall 2013 to Fall 2014 using a phased approach. Phase 1 included collecting and analyzing data from three study sites during late Fall 2013 into winter 2013. The purpose of Phase 1 was to test the developed field methodology and ensure that the data collected provides adequate resolution for calculating local rating curves. Phase 2 occurred during the Summer 2014 and included collecting field data from the remaining five study sites using a slightly updated data collection approach, compiling the field data and the alternate data sources, and developing the cross-sections' channel-floodplain topography and rating curves.

Materials & Methods

Site Selection

Site selection included vetting alluvial channel sites from the Regional Curve Study network and other known alluvial channel sites around the North Bay based on several site characteristics. The selected sites needed to have a relatively low channel gradient (reach-average slope ≤ 2.5%), have established floodplains (either intact or developed), be located at the bottom of a relatively moderate to large watershed (drainage area ≥ 1 mi^2), be without considerable hydraulic controls (e.g., weirs, undersized bridges and culverts), have a varying degree of channel complexity and disturbance, and be easily accessible with no permission issues. In addition, all sites had to have high resolution LiDAR data for use in comparing HCM approach output to topographic input data, and a few sites had to have flow gages nearby to enable comparison of HCM approach output to measured hydraulic conditions. Based on these criteria, we selected five sites from the Regional Curve Study network (Corte Madera Creek, Crane Creek, Lagunitas Creek, Miller Creek, and Novato Creek) and three additional North Bay sites known from previous SFEI studies (Browns Valley Creek, Salvador Creek, and Sulphur Creek) (Figure 1). Table 1 provides the relevant characteristics for each site selected.

Data Collection & Compilation

Study Reach Establishment

At each field site, we established a study reach that was homogeneous with respect to geomorphic characteristics and processes (i.e., consistent channel morphology with no considerable flow or sediment inputs or losses). To ensure adequate channel length necessary for developing reach-average hydraulic conditions, reaches were approximately 20 "bankfull widths" (or, presumed reach-average flow width during a 1.5- to 2-year flood event) in length and began and ended at major breaks in channel slope or at changes in channel geomorphic units (e.g., plane bed to pool-riffle). Within each study reach, we established three cross-section locations that represented local channel and floodplain

conditions: one cross-section towards the upstream end of the reach, one in the middle of the reach, and one towards the downstream end of the reach. At the gaged sites, the middle cross-section was placed at the location where the United States Geological Survey (USGS) monitors stage and measures discharge. We used a hand-held global positioning system (GPS) unit to record the location of reach boundaries (i.e., upstream and downstream boundary thalweg locations) and each cross-section thalweg location. Finally, the reach and each cross-section location were photo-documented in detail.

Cross-section Surveys

At each cross-section location, we conducted detailed topographic surveys through the active channel and part of the adjacent floodplain using an auto-level and stadia rod. The surveys extended approximately 100 ft into floodplains beyond channel edges or, when that was not possible, to the extent of allowable access. Ground surface elevations were recorded between the stakes every 1 to 3 ft using standard methodology (*cf*. Harrelson et al. 1994). We captured key geomorphic features such as the channel edges, the presumed bankfull flow water surface elevation, and the channel thalweg. We used a hand-held GPS unit to record the cross-section start and end locations.

Following the field effort, we entered the cross-section start and end locations into GIS. Floodplain elevations beyond the survey extent out to the presumed 50-year flood inundation extent were extracted from high resolution LiDAR data and then combined with the field survey data. This approach assumed that the LiDAR floodplain elevations closely match actual floodplain elevations at all the study cross-sections, which was based on a comparison of surveyed and LiDAR floodplain elevations at several study cross-sections.

Channel & Floodplain Roughness Assessments

At all cross-section locations, we used an intensive, field-based "composite" method to determine roughness values for the channel and adjacent floodplains. This method entailed adjusting a base roughness value with factors reflecting local physical conditions and using literature values for floodplain areas that could not be surveyed. At the three gaged study sites, we also calculated channel and floodplain roughness using a relatively simple method based on readily available information. This simple method, called the modified Strickler method, calculated bed roughness using a representative bed particle size with the Strickler (1923) equation and used literature values for floodplain roughness. Both methods are described in detail below.

Composite Method

Under the composite method, channel roughness ($n_{channel}$) was calculated below the channel edge on both banks using the Cowan (1956) equation:

$$n_{channel} = (n_b + n_1 + n_2 + n_3 + n_4)m$$

where;
n_b = base roughness value for a straight, uniform channel of natural materials,
n_1 = adjustment factor that accounts for surface irregularities,
n_2 = adjustment factor that accounts for variability in the channel cross-section shape,
n_3 = adjustment factor that accounts for obstructions,

n_4 = adjustment factor that accounts for vegetation and flow conditions, and
m = adjustment factor that accounts for channel meandering.

Following the channel roughness calculation approach presented in Aldridge and Garrett (1973), the channel base roughness (n_b) was determined at each cross-section as a function of local flow depth and bed texture using the Limerinos (1970) roughness equation:

$$n_b = \frac{(0.0926)(R^{1/6})}{1.16 + 2\log(\frac{R}{D_{84}})}$$

where;
R = hydraulic radius (similar to average flow depth, ft)
D_{84} = the bed particle size that is larger than 84% of the bed particles present (ft)

The hydraulic radius was derived from cross-section survey topography and D_{84} was derived from collected Wolman (1954) pebble count data. Pebble counts entailed measuring the intermediate axis (or b-axis) of 100 bed particles across the width of the active channel bed over an area that extended approximately 10 ft upstream and downstream of the cross-section. The pebble count data were then compiled into bed particle size distributions (i.e., plots of bed particle size vs. cumulative percent finer), from which cross-section specific D_{84} values were extracted.

Channel roughness adjustment factors (n_1 through n_4 and m) were determined for local channel conditions by combining field observations of channel physical conditions with a table of established channel roughness factor values (Table 2). Each channel roughness adjustment factor has a range of categories with a range of associated factor values, making value selection somewhat subjective and highly susceptible to user bias. To ensure consistency, each field staff member was trained in selecting appropriate channel roughness adjustment factor values and the same field team selected adjustment factors at each cross-section location.

Similar to the channel, the floodplain roughness ($n_{floodplain}$) for local conditions at each cross-section was calculated by combining a base roughness value and adjustment factors (Arcement and Schneider 1989). The equation used to calculate floodplain roughness was:

$$n_{floodplain} = (n_b + n_1 + n_2 + n_3)$$

where;
n_b = base roughness for the floodplain's natural bare surface,
n_1 = adjustment factor that accounts for surface irregularities,
n_2 = adjustment factor that accounts for vegetation type and density, and
n_3 = adjustment factor that accounts for obstructions.

However, unlike channel roughness, floodplain roughness was determined for individual floodplain areas that are distinct with respect to dominant roughness elements. For each individual floodplain area considered, base roughness and roughness adjustment factors were determined by combining observations of the floodplain conditions with tables of established roughness values (Tables 3 and 4).

Base roughness values were determined from a visual assessment of dominant floodplain surface substrate texture (or estimated median surface particle size [D_{50}] for coarse sand and larger), and roughness adjustment factor values were determined through a visual assessment of local floodplain conditions. The adjustment factor values selected were presumed to represent average conditions for floodplain inundation depths ranging from several inches to a few feet. As with the channel roughness assessment, the subjective nature of floodplain roughness determination required training field staff in base roughness and adjustment value selection. For floodplain areas beyond the topographic survey extent, roughness values were estimated extent using aerial imagery and field observations combined with commonly used land use-based literature roughness values (e.g., Chow 1959).

Modified Strickler Method

Similar to the composite method, the modified Strickler method for determining roughness involved calculating separate roughness values for the channel and the floodplains at each cross-section. Channel roughness for all flow depths was estimated from a single bed particle size using the Strickler (1923) equation:

$$n = 0.034\ (D_{50})^{1/6}$$

where;
D_{50} = the bed particle size that is larger than 50% of the bed particles present, or the median particle size (ft).

As with the D_{84} values used in the composite approach, the D_{50} values were determined from the compiled local particle size distributions.

Roughness values for the portion of the floodplain from the channel edge to the topographic survey extent were estimated using the same literature-based approach described above. These values were then combined with composite approach roughness values for the portion of the floodplain from the topographic survey extent to the presumed 50-year flood inundation extent.

Data Analysis

Following topographic and roughness data collection and compilation, we used the compiled data with Manning's equation to develop local relationships between discharge and flow stage, or rating curves, at each cross-section. Initial analysis focused on comparing calculated rating curves to USGS rating curves to assess the accuracy of rating curves calculated using an "intensive" field-based method roughness and a "simple" method roughness based on readily available information. At the three sites with USGS gaging stations, we calculated two rating curves at the middle cross-section. The first rating curve was based on field-derived channel topography with supplemental LiDAR floodplain topography and roughness estimates using the intensive composite method. The second rating curve was based on field-derived channel topography with supplemental LiDAR floodplain topography and roughness estimates using the simpler modified Strickler method. We then compared the calculated rating curves to USGS gage rating curves to determine the overall degree of agreement and the need for site-specific channel roughness "scaling factors" that improve rating curve agreement. Rating curve agreement at each gage was determined by averaging the ratios of USGS discharge values and calculated discharge values for the

range of flow stages covered by the USGS rating curve. The USGS and calculated rating curves were considered to be at an acceptable degree of agreement when the average of the ratio values was ≥0.9.

For the HCM approach to be useful in a desktop tool, it should output similar rating curves using elevations derived from a detailed field survey or from high-resolution LiDAR data. However, as LiDAR data can vary considerably due to vegetation and water interference, it was necessary to compare rating curves using field survey topography and LiDAR topography to assess the overall utility of North Bay LiDAR data. At all 24 cross-section locations, rating curves were calculated using the composite method roughness with a regional scaling factor (i.e., the average of the scaling factors from the three gaged sites) combined with: 1) field-derived channel topography supplemented with LiDAR floodplain topography; and 2) LiDAR channel and floodplain topography. The two rating curves for each cross-section were then compared to determine the overall degree of agreement. Similar to the comparison of calculated rating curves to measured rating curves, rating curve agreement was determined using the average ratio of the two rating curve discharge values for a range of flow stages. A ratio value >0.66 indicated a high degree of agreement, a value between 0.66 and 0.33 indicated a medium degree of agreement, and a value <0.33 indicated a low degree of agreement.

Results

This section focuses on summarizing the results from comparing rating curves at all of the study cross-sections. The physical data used to calculate the cross-section rating curves can be found in Appendix A and the cross-section topography and calculated rating curves can be found in Appendix B.

Comparison of Calculated & USGS Rating Curves

Comparisons of USGS rating curves to calculated rating curves using roughness values derived from the intensive composite method and the simpler modified Strickler method are shown in Figures 2 through 4. These figures also show the stages for the 2-year, 10-year, and 50-year flood events and the stage associated with initial floodplain inundation ($Q_{top\text{-}of\text{-}bank}$). Both calculated rating curves at all three gaged sites required channel roughness scaling factors to improve the agreement with USGS curves and arrive at an average discharge ratio value near 0.9. The scaling factors for the rating curves derived using the composite method roughness values ranged from 0.26 to 0.53 (i.e., calculated roughness was too high) while the scaling factors for the rating curves derived using the modified Strickler method roughness values ranged from 1.3 to 1.7 (i.e., calculated roughness was too low). The variability among the scaling factors using the modified Strickler method was somewhat lower than the scaling factors for the rating curves using the composite method, suggesting the modified Strickler method may be more universal. However, it is important to note that the cause for the scaling factor variability among the gaged sites is currently not known but could be related to important elements not explicitly accounted for in channel roughness determination such as local channel gradient.

Figures 2 through 4 are also important in showing the range of flows for which the scaled calculated rating curves agree with USGS rating curves (i.e., the calibrated sections of the calculated rating curves). To have confidence that the calculated rating curves are capturing the desired flooding dynamics, they should be calibrated for flows ranging from the 2-year flow up to the 50-year flood event. All three USGS rating curves include high flows at or near the predicted 100-year flood event, giving confidence that the

gage-specific roughness scaling factors provide calibrated rating curves for the flows of interest in this study.

Comparison of Calculated Rating Curves Using Field-based and LiDAR Topography

Results from comparing the two calculated rating curves at each study cross-section are summarized in Table 5. Over two-thirds of the cross-sections had a high level of rating curve agreement and only one of the 24 cross-sections had a low level of agreement. Most of the sites had two of three cross-sections with a high level of rating curve agreement, with the exceptions being the Browns Valley Creek, Sulphur Creek, and Novato Creek sites. For Browns Valley Creek and Sulphur Creek, the cause of the medium degree of rating curve agreement is not consistent. LiDAR data at these sites show a wider and/or deeper channel compared to field data in some instances and a narrower and/or shallower channel in others. The degree of agreement could therefore be related to either issues with the LiDAR (e.g., data filtering) or issues with our analysis (e.g., generating LiDAR channel topography at the exact same location as the field survey). For Novato Creek, the low degree and medium degree of rating curve agreement at two of the three cross-sections appears to be primarily driven by the LiDAR channel elevations being higher on one bank than the field survey elevations. This suggests the Novato Creek channel likely scoured in the years between the LiDAR and field data collection efforts. These bank elevation differences highlight the importance of having a general understanding of channel morphologic change since LiDAR data collection as a means of determining LiDAR data utility for assessing current hydraulic conditions.

Discussion

Synthesis

The goals of this study were to validate the HCM approach for determining local flow hydraulics and associated flooding extent, and to assess the effects of input data source on the HCM approach output. The results presented in this report show that the approach has been validated for North Bay watersheds and that input data derived from intensive field data and from more readily available data sources can provide similar results. The specific answers to the two research questions driving this study are as follows:

1. Does the HCM approach adequately predict local hydraulic conditions for a range of flood flows using intensive field data?

   Yes. At the cross-sections located next to USGS gages, the study results show that the rating curves calculated using the intensive, field-based composite method roughness values closely matched the USGS rating curves when a roughness scaling factor was applied. At all three gage sites, applying the scaling factor resulted in an overall excellent degree of rating curve agreement (average ratio of USGS values to calculated values were ≥ 0.9), with the rating curves spanning low discharges all the way up to the predicted 100-year flood discharge.

2. Do readily available alternate or remote data sources provide similar results as intensive field data?

Yes. At the three gaged study cross-sections, the rating curves calculated using the modified Strickler method roughness values (i.e., values derived from just the median bed particle size and a general assessment of floodplain land use) with a scaling factor had the same degree of agreement with the USGS rating curve as the scaled rating curve calculated using the intensive composite method roughness values. In addition, comparing rating curves calculated using field surveyed topography and LiDAR topography at all 24 study cross-sections showed that LiDAR data consistently provided similar rating curves as those generated using ground survey data. The overall high degree of agreement between the calculated rating curves for a vast majority of representative North Bay channel cross-sections gives confidence that Marin, Napa, and Sonoma County LiDAR datasets are appropriate for use within the HCM.

This study also elucidated the overall utility of the HCM approach for estimating flooding extent in low-lying alluvial channels and the important characteristics that should be considered when using the approach. The study showed the following:

- Efficiency for developing a functional riparian area estimate (i.e., how difficult is it for the average person to use?)

  The HCM approach should be used by scientists and planners with at least a basic understanding of flow hydraulics, fluvial geomorphology, and riparian ecology. The user should be familiar with Manning's equation, be able to obtain site topographic data (either through a field survey or from LiDAR data), be able to obtain site channel and floodplain roughness values (through a field survey, simple equations, literature values, or a combination), and be proficient with spreadsheet and GIS software.

- Ease of use for developing a functional riparian area estimate (i.e., how many inputs are necessary and how complex are the inputs?)

  The HCM approach is very easy to use for developing an estimate of functional riparian extent in low gradient alluvial channels. The required inputs are channel-floodplain cross-section topography, local channel slope through the cross-section, and roughness estimates for the channel and adjacent floodplains. Our analyses suggest that in North Bay watersheds, LiDAR data can be used for channel-floodplain topography and channel roughness can be estimated using an estimate of median bed particle size with a scaling factor. These input values are readily obtainable and easily entered into the analysis for predicting flooding extent and associated functional riparian area extent.

- Key considerations when using the HCM approach (i.e., what were the important lessons learned during assessment and testing?)

  This study highlighted two key factors that need to be considered when using the HCM approach. First, the study results show that rating curves generated using LiDAR topography and field survey topography were very similar at most, but not all, of the 24 study cross-sections. This highlights the fact that LiDAR data should not be automatically assumed to be a good

representation of current field conditions and that the user needs to have a general understanding of factors that could be causing disagreement between LiDAR and field data (e.g., data filtering, channel change following LiDAR data collection). Second, the study results show that channel roughness estimates determined from either the intensive composite method or the simpler modified Strickler method need to be scaled in order to reflect actual field conditions. When using these methods to develop channel roughness, the user needs to account for the scaling factors when developing local rating curves.

- Overall HCM approach advantages and disadvantages

  The main advantage of the HCM approach is that it is a relatively simple approach that can provide flooding extent estimates for a range of flows with only a few easily obtainable input variables. Conversely, the main disadvantages of the approach are that it assumes that the channel is essentially in a state of quasi-equilibrium (i.e., the cross-section flow area and/or slope are not actively adjusting) and it does not account for hydraulic complexities like bridge constrictions when calculating local rating curves and flooding extents. However, as the HCM is intended to be a planning-level tool, its simple approach seems well-suited for providing a general sense of functional riparian area extent in most landscape settings.

Recommended Next Steps

Although the data collected and compiled during this study were sufficient for validating the HCM approach and assessing the effects of input data sources on output, additional data collection efforts and quantitative analyses are necessary for improving the performance of the HCM approach in North Bay watersheds and elsewhere around the state. Recommended future data collection efforts and quantitative analyses include the following:

- **Additional comparisons of calculated rating curves and gage rating curves in the North Bay**. Continuing to compare calculated rating curves with gage rating curves could help clarify the specific factors driving the degree of agreement (e.g., local slope impacts on roughness values) and could help with the development of a method for determining roughness scaling factors at any North Bay alluvial channel location.

- **Compare calculated and gage rating curves and the utility of LiDAR topography in other regions of California**. Conducting the analyses done for this study in other hydrologic regions around the state could help clarify the factors driving the degree of rating curve agreement, help develop a method for determining regional roughness scaling factors for additional regions, and help determine which LiDAR datasets around the state are suitable for use within HCM.

- **Investigate additional methods for determining channel roughness**. The results from this study showed that rating curves calculated using roughness values derived from a simple equation matched gage rating curves when a scaling factor was applied. As channel roughness can be

calculated a variety of ways using a range of variables, future work could focus on testing several methods for calculating channel roughness with the goal of finding the simplest method that gives a channel roughness and associated rating curve that most closely matches a gage rating curve.

References

Aldridge, B.N., and J. M. Garrett. 1973. Roughness coefficients for stream channels in Arizona: U.S. Geological Survey Open-File Report, 87 p.

Arcement , G.J., Jr. and V.R. Schneider. 1989. Guide for selecting Manning's roughness coefficients for natural channels and flood plains. U.S. Geological Survey Water Supply Paper 2339, 38 p.

Benson, M.A. and T. Dalrymple. 1967. General field and office procedures for indirect discharge measurements. U.S. Geological Survey Techniques for Water-Resources Investigations, Book 3, Chapter A1, 30 p.

Chow, V.T. 1959. Open Channel Hydraulics. McGraw Hill, New York.

Collins, L. and R. Leventhal. 2013. Regional curves of hydraulic geometry for wadeable Streams in Marin and Sonoma counties, San Francisco Bay Area. Data Summary Report.

Cowan, W.L.1956. Estimating hydraulic roughness coefficients. Agricultural Engineering, 37(7):473-475.

Harrelson, C. C., C. L. Rawlins, and J. P. Potyondy. 1994. Stream channel reference sites: an illustrated guide to field technique. General Technical Report RM-245. Prepared by USDA Forest Service, Rocky Mountain Forest and Range Experiment Station, Fort Collins, Colorado.

Ilhardt, B.L., E.S. Verry and B.J. Palik. 2000. Defining Riparian Areas. In: Verry, E.S., J.W. Hornbeck and C.A.Dolloff (eds.). Riparian Management in Forests of the Continental Eastern United States. Lewis Publishers, New York, 23-42.

Limerinos, J.T. 1970. Determination of the Manning coefficient from measured bed roughness in natural channels. U.S. Geological Survey Water Supply Paper 1898-B, 47p.

Strickler A.1923. Beiträge zur Frage der Geschwindigkeitsformel und der Rauhigkeitszahlen fur Ströme, Kanäle und Geschlossene Leitungen, Berna.

Wolman, G. M. 1954. A method of sampling coarse river-bed material. Transactions of the American Geophysical Union, 35: 951–956.

Figure 1. Study site locations

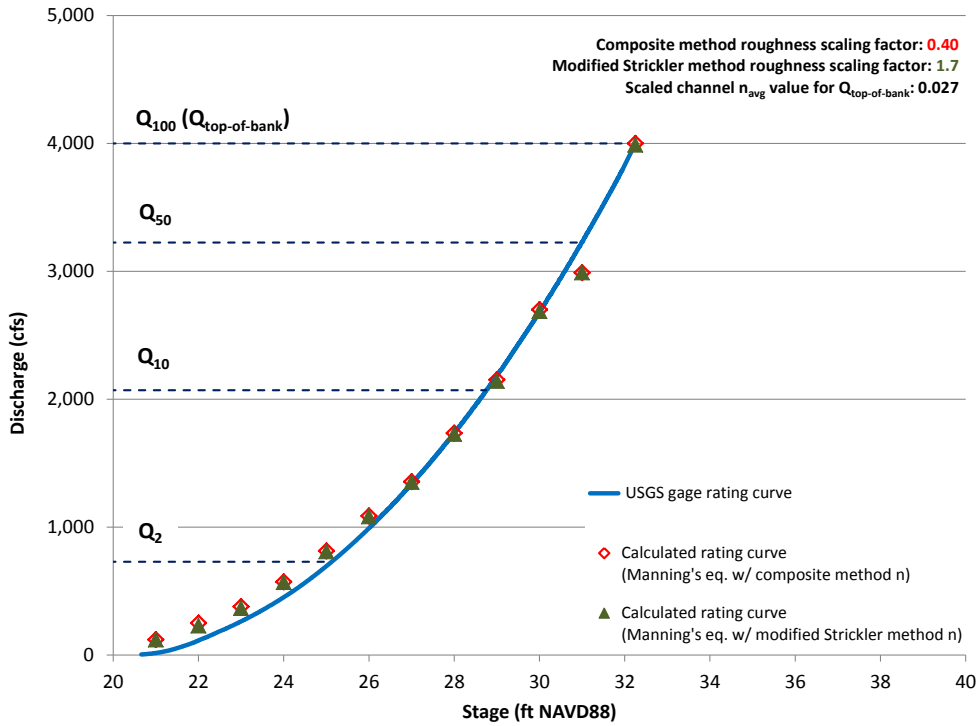

Figure 2. Comparison of USGS and calculated rating curves at the Novato Creek site.

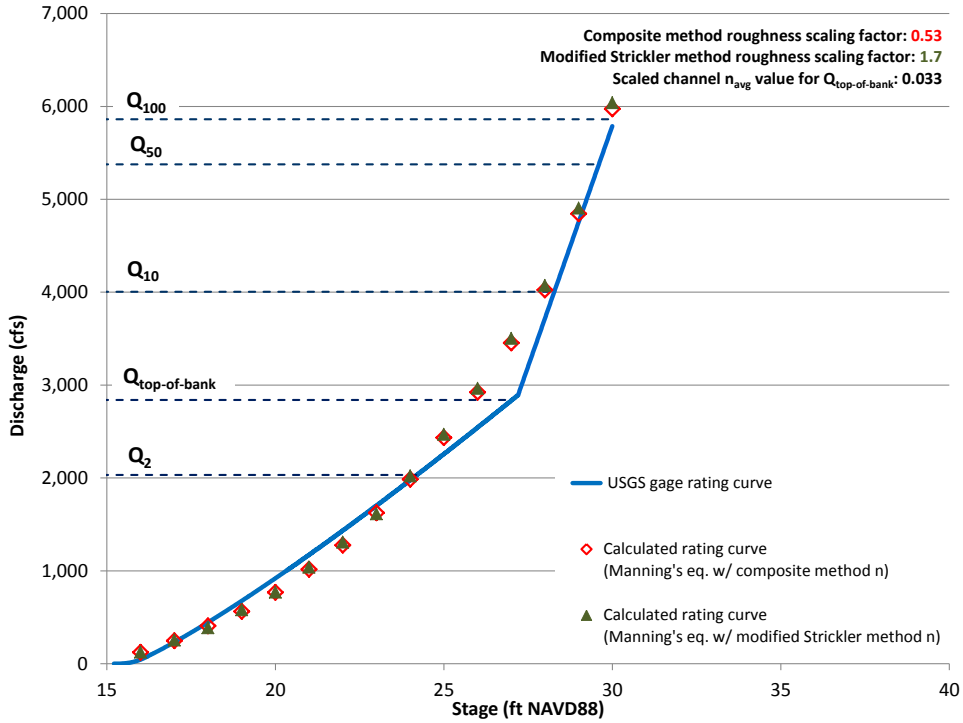

Figure 3. Comparison of USGS and calculated rating curves at the Corte Madera Creek site.

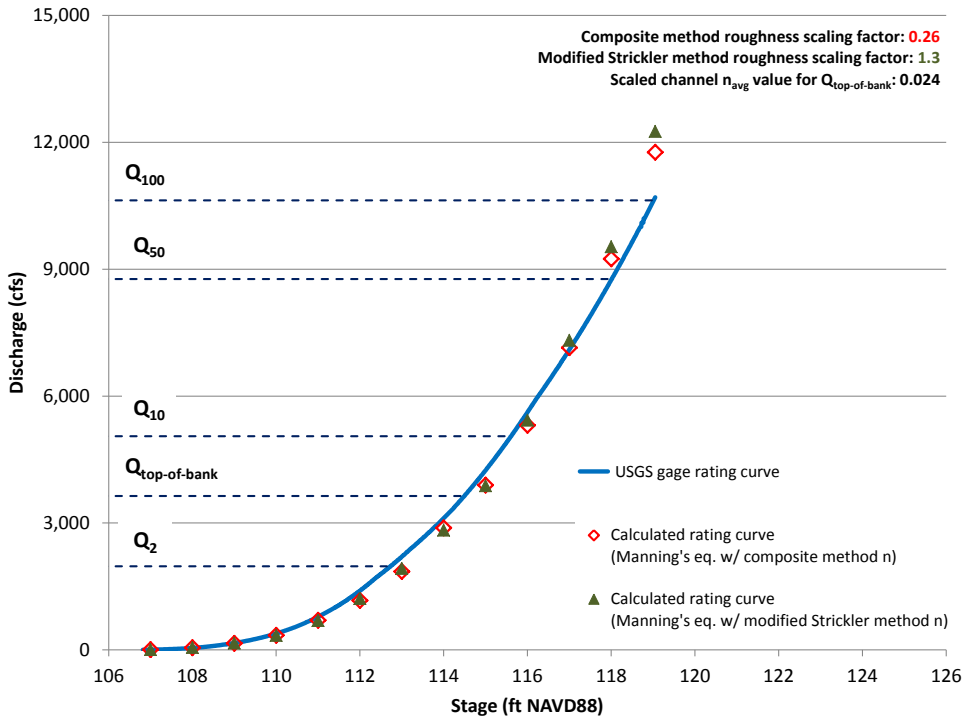

Figure 4. Comparison of USGS and calculated rating curves at the Lagunitas Creek site.

Table 1. Relevant characteristics for the selected study sites.

Phase	Study site	County	Watershed Size (mi^2)	Reach-average channel slope	Relative degree of channel complexity (H, M, L)	Relative degree of riparian vegetation disturbance (H, M, L)	Flow gage present
1	Miller Cr.	Marin	6.4	0.005	M	M	No
	Novato Cr.	Marin	9.6[a]	0.004	M	M	Yes
	Crane Cr.	Sonoma	2.1	0.024	M	H	No
2	Corte Madera Cr.	Marin	16.8[a]	0.004	L	M	Yes
	Lagunitas Cr.	Marin	12.8[a]	0.005	H	M	Yes
	Browns Valley Cr.	Napa	2.7	0.008	H	M	No
	Salvador Cr.	Napa	3.5	0.002	L	H	No
	Sulphur Cr.	Napa	9.2	0.007	M	M	No

[a] Area downstream of large dams

Table 2. Channel roughness adjustment factor values (from Arcement and Schneider 1989)

Channel conditions		*n* value adjustment[1]	Example
Degree of irregularity (n_1)	Smooth	0.000	Compares to the smoothest channel attainable in a given bed material.
	Minor	0.001–0.005	Compares to carefully dredged channels in good condition but having slightly eroded or scoured side slopes.
	Moderate	0.006–0.010	Compares to dredged channels having moderate to considerable bed roughness and moderately sloughed or eroded side slopes.
	Severe	0.011–0.020	Badly sloughed or scalloped banks of natural streams; badly eroded or sloughed sides of canals or drainage channels; unshaped, jagged, and irregular surfaces of channels in rock.
Variation in channel cross section (n_2)	Gradual	0.000	Size and shape of channel cross sections change gradually.
	Alternating occasionally	0.001–0.005	Large and small cross sections alternate occasionally, or the main flow occasionally shifts from side to side owing to changes in cross-sectional shape.
	Alternating frequently	0.010–0.015	Large and small cross sections alternate frequently, or the main flow frequently shifts from side to side owing to changes in cross-sectional shape.
Effect of obstruction (n_3)	Negligible	0.000–0.004	A few scattered obstructions, which include debris deposits, stumps, exposed roots, logs, piers, or isolated boulders, that occupy less than 5 percent of the cross-sectional area.
	Minor	0.005–0.015	Obstructions occupy less than 15 percent of the cross-sectional area, and the spacing between obstructions is such that the sphere of influence around one obstruction does not extend to the sphere of influence around another obstruction. Smaller adjustments are used for curved smooth-surfaced objects than are used for sharp-edged angular objects.
	Appreciable	0.020–0.030	Obstructions occupy from 15 to 50 percent of the cross-sectional area, or the space between obstructions is small enough to cause the effects of several obstructions to be additive, thereby blocking an equivalent part of a cross section.
	Severe	0.040–0.050	Obstructions occupy more than 50 percent of the cross-sectional area, or the space between obstructions is small enough to cause turbulence across most of the cross section.
Amount of vegetation (n_4)	Small	0.002–0.010	Dense growths of flexible turf grass, such as Bermuda, or weeds growing where the average depth of flow is at least two times the height of the vegetation; supple tree seedlings such as willow, cottonwood, arrowweed, or saltcedar growing where the average depth of flow is at least three times the height of the vegetation.
	Medium	0.010–0.025	Turf grass growing where the average depth of flow is from one to two times the height of the vegetation; moderately dense stemmy grass, weeds, or tree seedlings growing where the average depth of flow is from two to three times the height of the vegetation; brushy, moderately dense vegetation, similar to 1- to 2-year-old willow trees in the dormant season, growing along the banks, and no significant vegetation is evident along the channel bottoms where the hydraulic radius exceeds 2 ft.
	Large	0.025–0.050	Turf grass growing where the average depth of flow is about equal to the height of the vegetation; 8- to 10-year-old willow or cottonwood trees intergrown with some weeds and brush (none of the vegetation in foliage) where the hydraulic radius exceeds 2 ft; bushy willows about 1 year old intergrown with some weeds along side slopes (all vegetation in full foliage), and no significant vegetation exists along channel bottoms where the hydraulic radius is greater than 2 ft.
	Very large	0.050–0.100	Turf grass growing where the average depth of flow is less than half the height of the vegetation; bushy willow trees about 1 year old intergrown with weeds along side slopes (all vegetation in full foliage), or dense cattails growing along channel bottom; trees intergrown with weeds and brush (all vegetation in full foliage).
Degree of meandering[2] (m)	Minor	1.00	Ratio of the channel length to valley length is 1.0 to 1.2.
	Appreciable	1.15	Ratio of the channel length to valley length is 1.2 to 1.5.
	Severe	1.30	Ratio of the channel length to valley length is greater than 1.5.

[1] Adjustments for degree of irregularity, variations in cross section, effect of obstructions, and vegetation are added to the base *n* value (table 1) before multiplying by the adjustment for meander.

[2] Adjustment values apply to flow confined in the channel and do not apply where downvalley flow crosses meanders.

Table 3. Base roughness values for channels and floodplains (from Arcement and Schneider 1989)

Bed material	Median size of bed material (in millimeters)	Base *n* value: Straight uniform channel[1]	Base *n* value: Smooth channel[2]
Sand channels			
Sand[3]	0.2	0.012	—
	.3	.017	—
	.4	.020	—
	.5	.022	—
	.6	.023	—
	.8	.025	—
	1.0	.026	—
Stable channels and flood plains			
Concrete	—	0.012–0.018	0.011
Rock cut	—	—	.025
Firm soil	—	0.025–0.032	.020
Coarse sand	1–2	0.026–0.035	—
Fine gravel	—	—	.024
Gravel	2–64	0.028–0.035	—
Coarse gravel	—	—	.026
Cobble	64–256	0.030–0.050	—
Boulder	>256	0.040–0.070	—

[1] Benson and Dalrymple (1967).
[2] For indicated material; Chow (1959).
[3] Only for upper regime flow where grain roughness is predominant.

Table 4. Floodplain roughness adjustment factor values (modified from Arcement and Schneider 1989)

Flood-plain conditions		*n* value adjustment	Example
Degree of irregularity (n_1)	Smooth	0.000	Compares to the smoothest, flattest flood plain attainable in a given bed material.
	Minor	0.001–0.005	Is a flood plain slightly irregular in shape. A few rises and dips or sloughs may be visible on the flood plain.
	Moderate	0.006–0.010	Has more rises and dips. Sloughs and hummocks may occur.
	Severe	0.011–0.020	Flood plain very irregular in shape. Many rises and dips or sloughs are visible. Irregular ground surfaces in pastureland and furrows perpendicular to the flow are also included.
Effect of obstructions (n_2)	Negligible	0.000–0.004	Few scattered obstructions, which include debris deposits, stumps, exposed roots, logs, or isolated boulders, occupy less than 5 percent of the cross-sectional area.
	Minor	0.005–0.019	Obstructions occupy less than 15 percent of the cross-sectional area.
	Appreciable	0.020–0.030	Obstructions occupy from 15 to 50 percent of the cross-sectional area.
Amount of vegetation (n_3)	Small	0.001–0.010	Dense growth of flexible turf grass, such as Bermuda, or weeds growing where the average depth of flow is at least two times the height of the vegetation, or supple tree seedlings such as willow, cottonwood, arrowweed, or saltcedar growing where the average depth of flow is at least three times the height of the vegetation.
	Medium	0.011–0.025	Turf grass growing where the average depth of flow is from one to two times the height of the vegetation, or moderately dense stemmy grass, weeds, or tree seedlings growing where the average depth of flow is from two to three times the height of the vegetation; brushy, moderately dense vegetation, similar to 1- to 2-year-old willow trees in the dormant season.
	Large	0.025–0.050	Turf grass growing where the average depth of flow is about equal to the height of the vegetation, or 8- to 10-year-old willow or cottonwood trees intergrown with some weeds and brush (none of the vegetation in foliage) where the hydraulic radius exceeds 2 ft, or mature row crops such as small vegetables, or mature field crops where depth of flow is at least twice the height of the vegetation.
	Very large	0.050–0.100	Turf grass growing where the average depth of flow is less than half the height of the vegetation, or moderate to dense brush, or heavy stand of timber with few down trees and little undergrowth where depth of flow is below branches, or mature field crops where depth of flow is less than the height of the vegetation.
	Extreme	0.100–0.200	Dense bushy willow, mesquite, and saltcedar (all vegetation in full foliage), or heavy stand of timber, few down trees, depth of flow reaching branches.

Table 5. Degree of agreement between the calculated rating curves using field-derived and LiDAR topography at each study site cross-section

Study site	Cross-section[a]	Avg. ratio of rating curve discharge values[b]	Degree of agreement[c]
Miller Cr.	1	0.57	Medium
	2	0.82	High
	3	0.69	High
Novato Cr.	1	0.88	High
	2	0.31	Low
	3	0.46	Medium
Crane Cr.	1	0.70	High
	2	0.86	High
	3	0.77	High
Corte Madera Cr.	1	0.87	High
	2	0.49	Medium
	3	0.91	High
Lagunitas Cr.	1	0.86	High
	2	0.68	High
	3	0.70	High
Browns Valley Cr.	1	0.68	High
	2	0.63	Medium
	3	0.53	Medium
Salvador Cr.	1	0.73	High
	2	0.79	High
	3	0.70	High
Sulphur Cr.	1	0.69	High
	2	0.64	Medium
	3	0.35	Medium

[a] The cross-section numbering increases downstream at all sites except Novato Cr.

[b] Average of values for the range of stages covered by the USGS rating curve

[c] An average ratio value >0.66 indicates a high degree of agreement, a value between 0.66 and 0.33 indicates a medium degree of agreement, and a value <0.33 indicates a low degree of agreement

Appendix A

Study Site Channel Geomorphic Data

Table A1. Site geomorphic data used to calculate local rating curves

Study site	Cross-section[a]	D_{50}[b] (mm)	D_{84}[b] (mm)	Channel slope through the cross-section[c]
Miller Cr.	1	9	24	0.004
	2	21	47	0.005
	3	7	16	0.005
Novato Cr.	1	11	34	0.004
	2	3	7	0.002
	3	19	45	0.0009
Crane Cr.	1	57	210	0.024
	2	32	92	0.022
	3	29	110	0.029
Corte Madera Cr.	1	11	28	0.002
	2	10	26	0.0007
	3	9	26	0.006
Lagunitas Cr.	1	11	26	0.003
	2	9	101	0.007
	3	14	36	0.004
Browns Valley Cr.	1	10	42	0.007
	2	6	25	0.010
	3	7	19	0.013
Salvador Cr.	1	9	34	0.001
	2	6	21	0.001
	3	10	48	0.005
Sulphur Cr.	1	4	14	0.008
	2	7	31	0.007
	3	11	30	0.007

[a] The cross-section numbering increases downstream at all sites except Novato Cr.

[b] Value derived from the pebble counts conducted at the cross-section

[c] Value derived from LiDAR elevation data

Appendix B

Study Site Cross-section Topography & Local Rating Curves

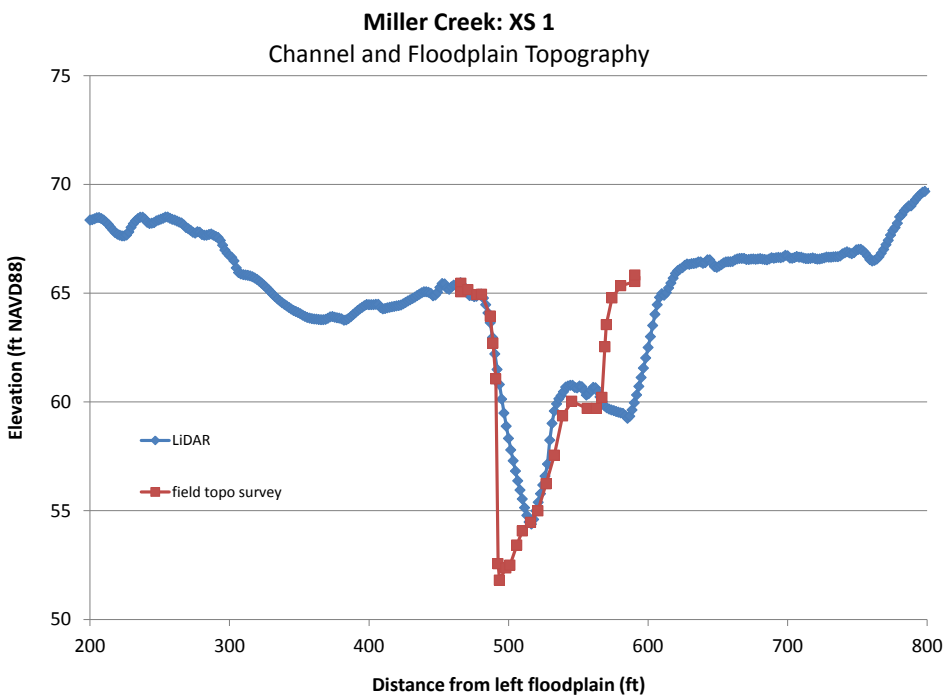

Figure B1. Miller Creek, cross-section 1 – LiDAR and field survey topography

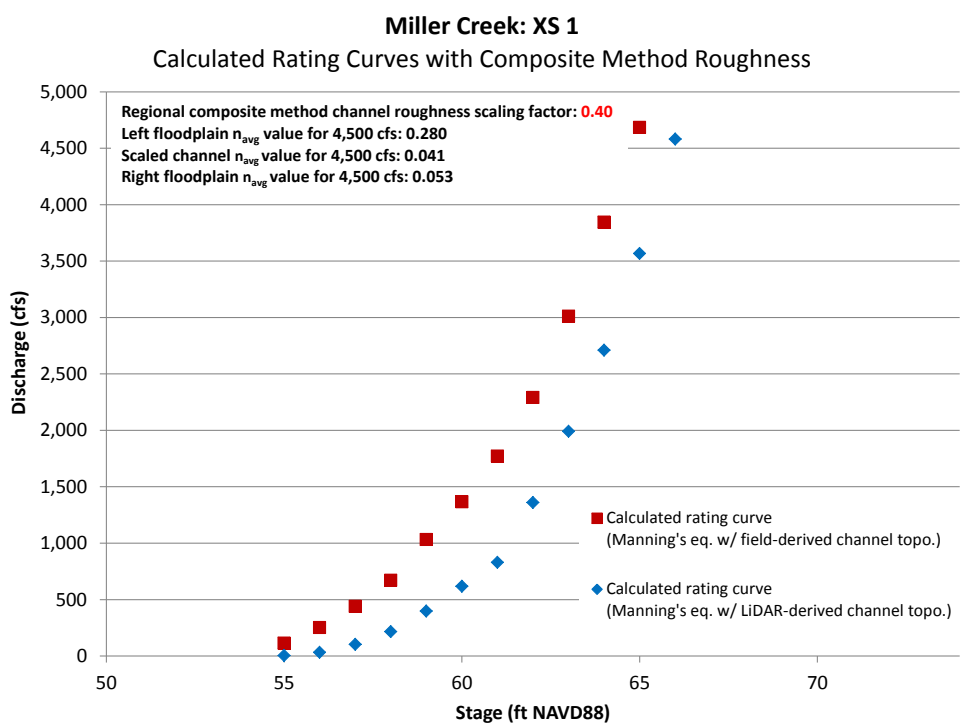

Figure B2. Miller Creek, cross-section 1 – calculated rating curves

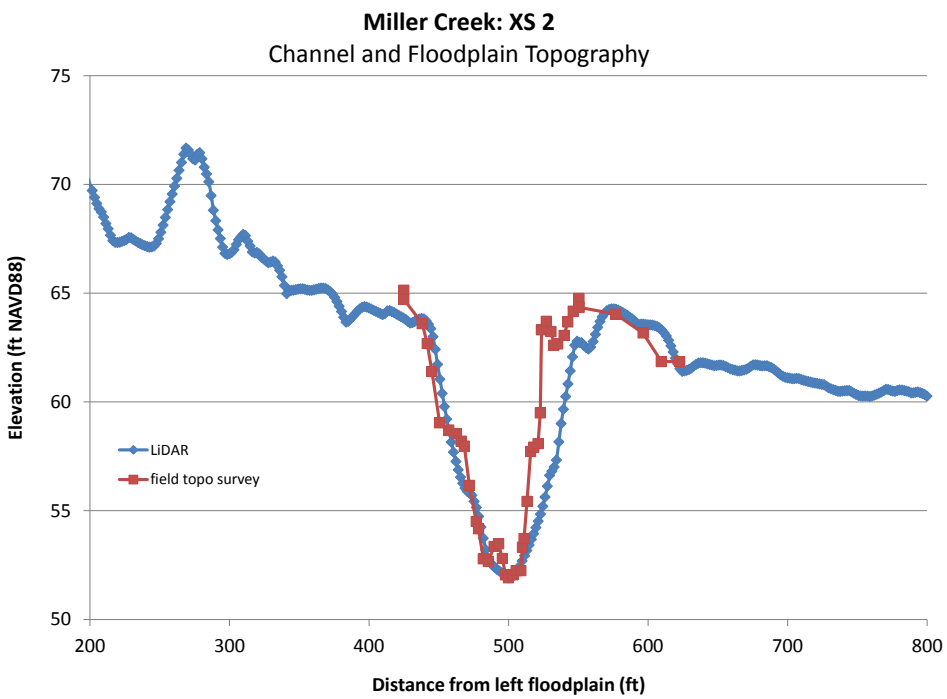

Figure B.3 Miller Creek, cross-section 2 – LiDAR and field survey topography

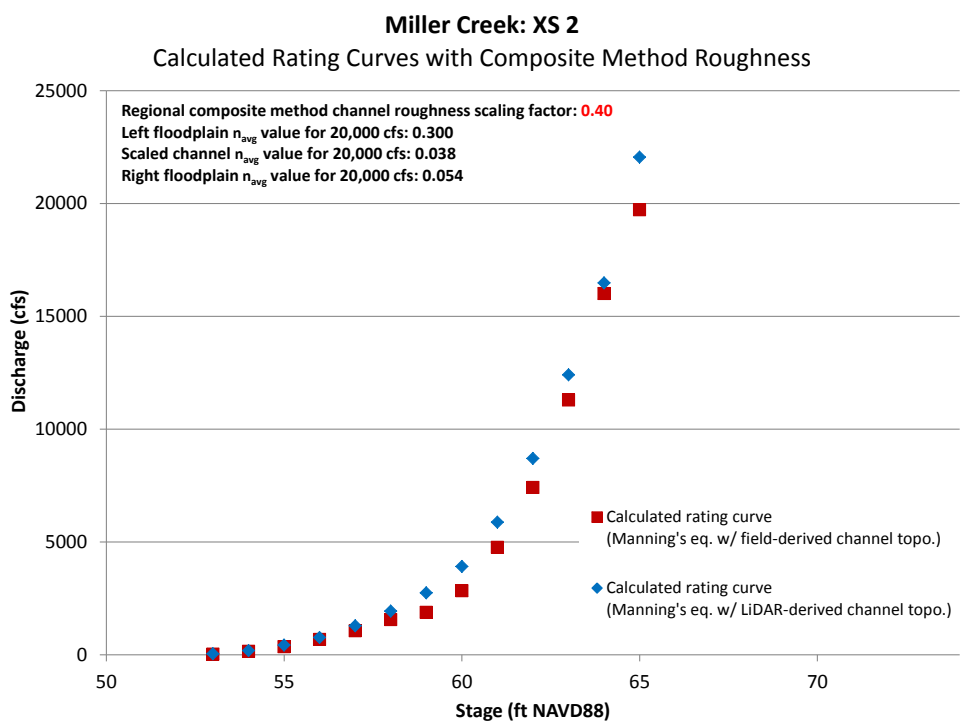

Figure B.4 Miller Creek, cross-section 2 – calculated rating curves

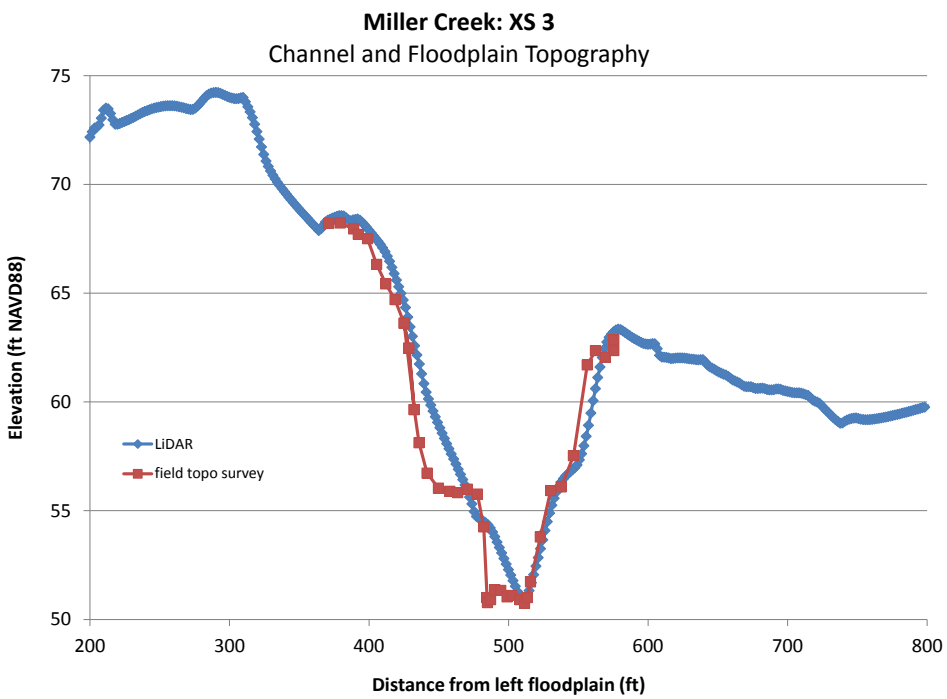

Figure B.5 Miller Creek, cross-section 3 – LiDAR and field survey topography

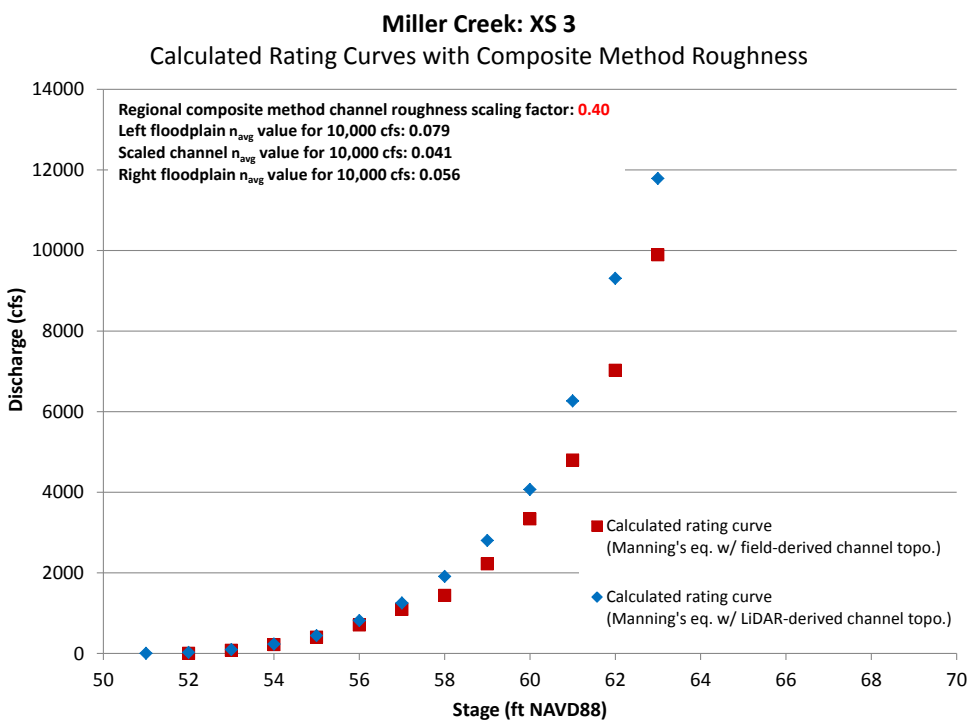

Figure B6. Miller Creek, cross-section 3 – calculated rating curves

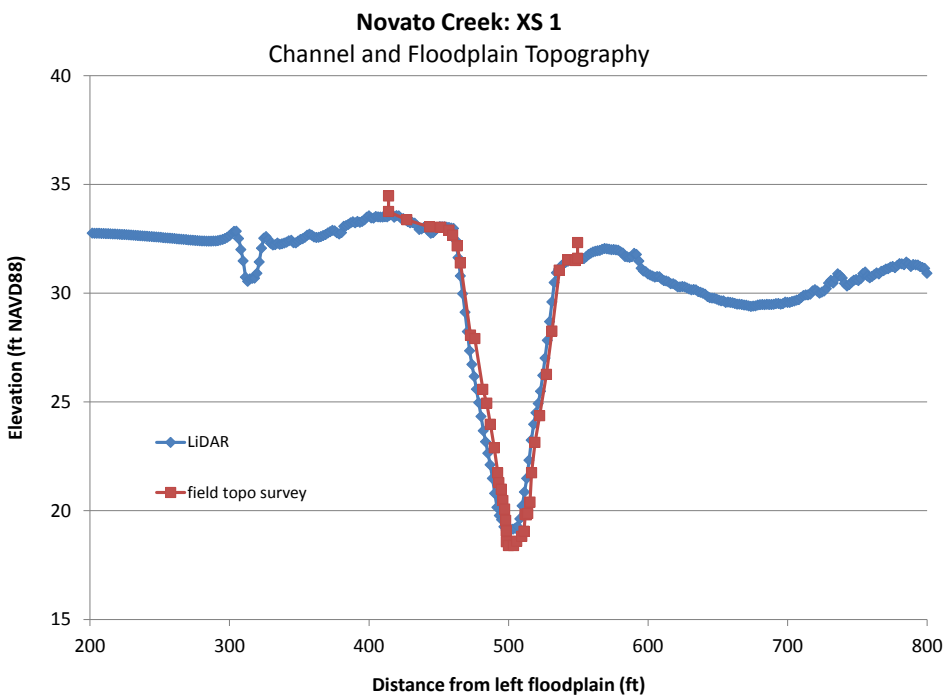

Figure B7. Novato Creek, cross-section 1 – LiDAR and field survey topography

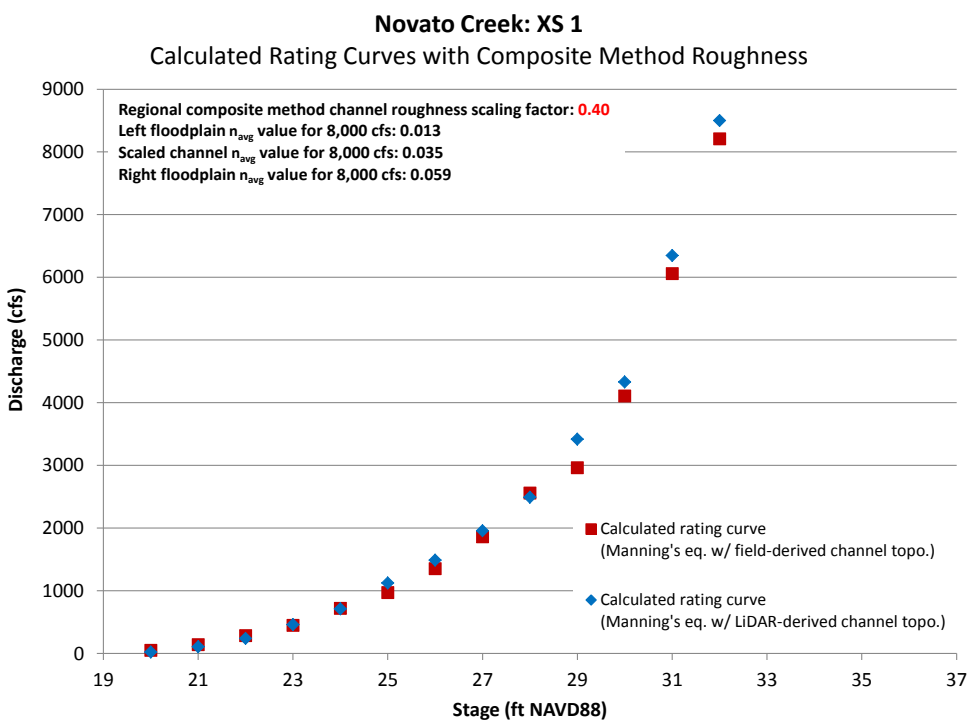

Figure B8. Novato Creek, cross-section 1 – calculated rating curves

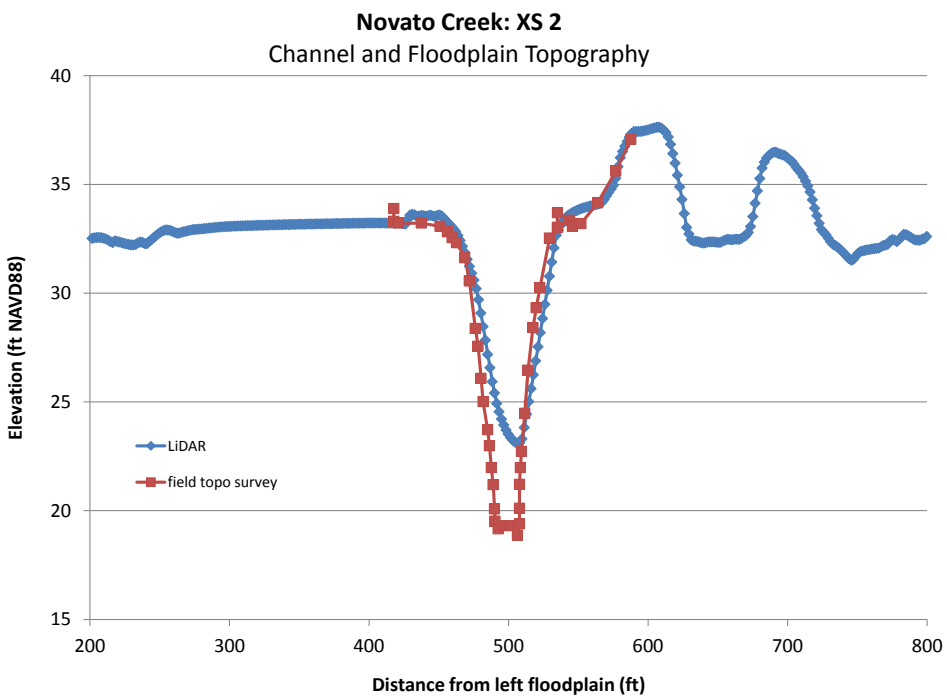

Figure B9. Novato Creek, cross-section 2 – LiDAR and field survey topography

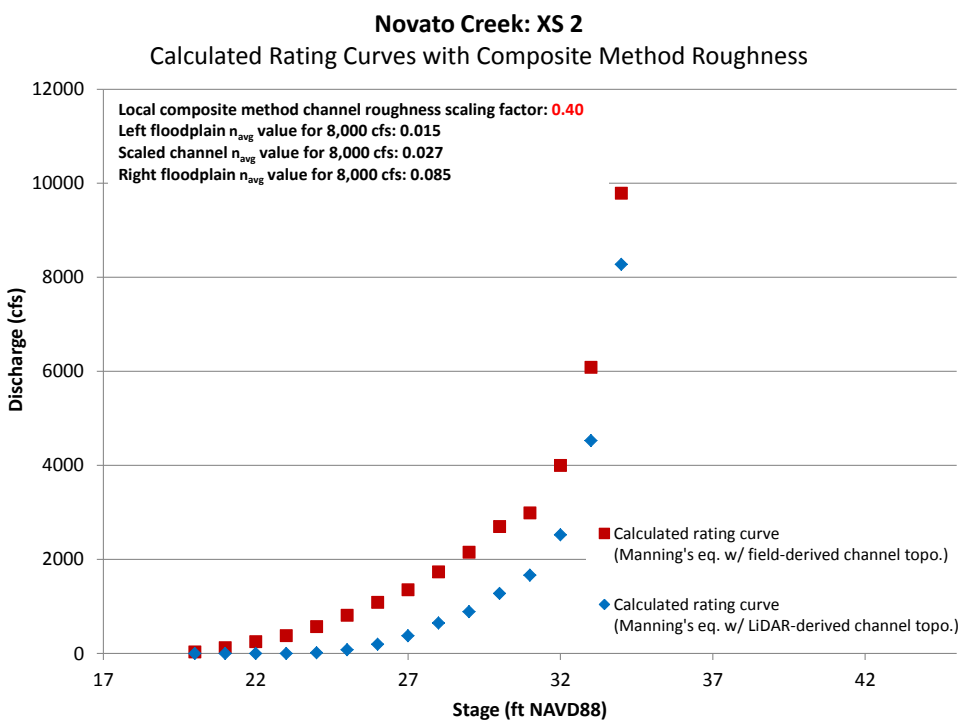

Figure B10. Novato Creek, cross-section 2 – calculated rating curves

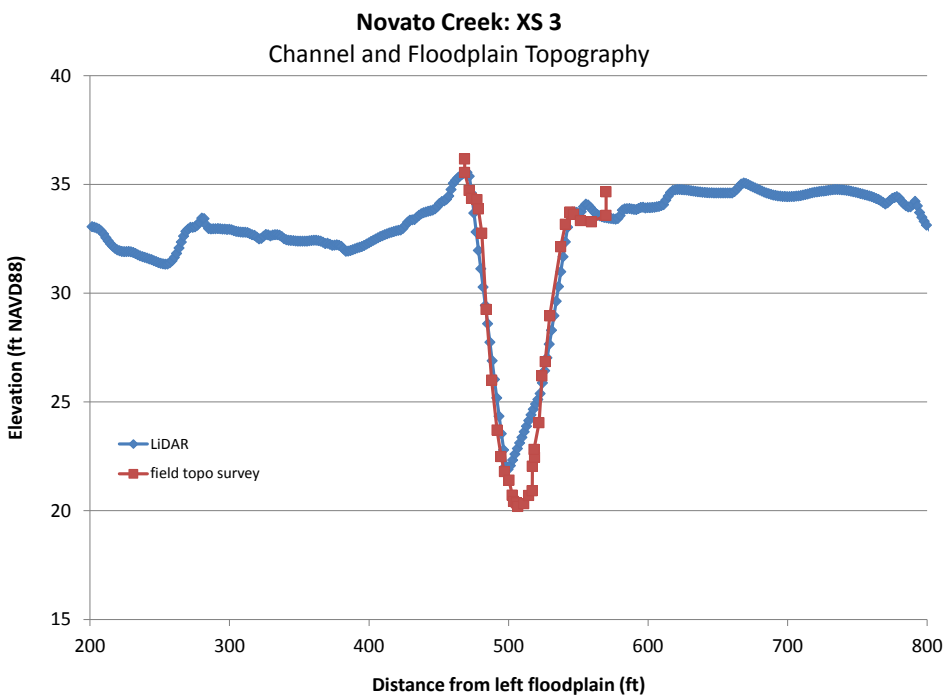

Figure B11. Novato Creek, cross-section 3 – LiDAR and field survey topography

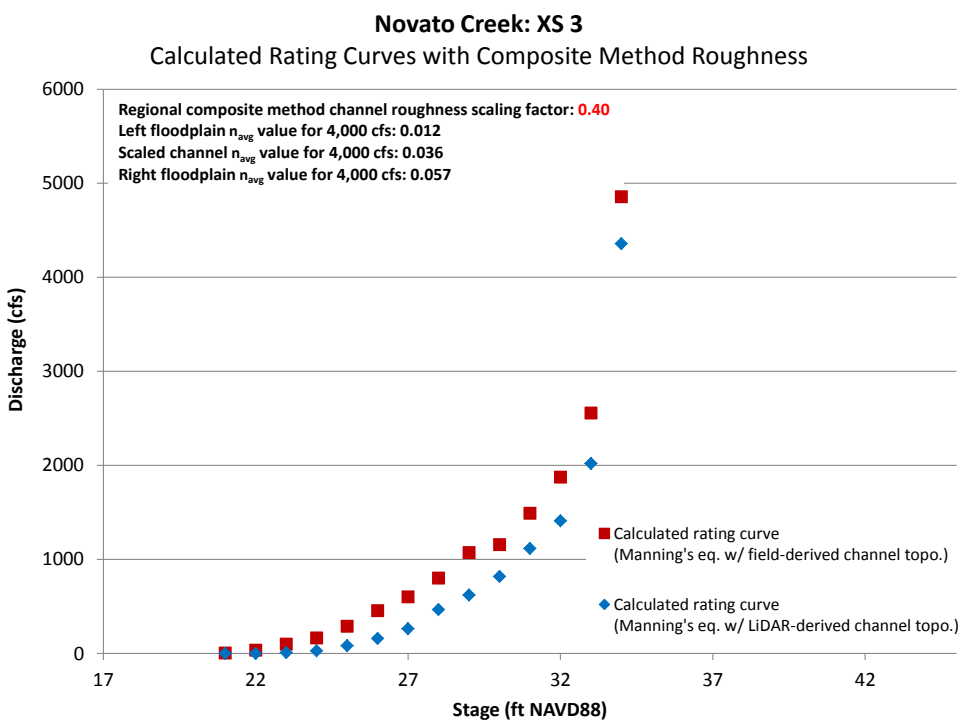

Figure B12. Novato Creek, cross-section 3 – calculated rating curves

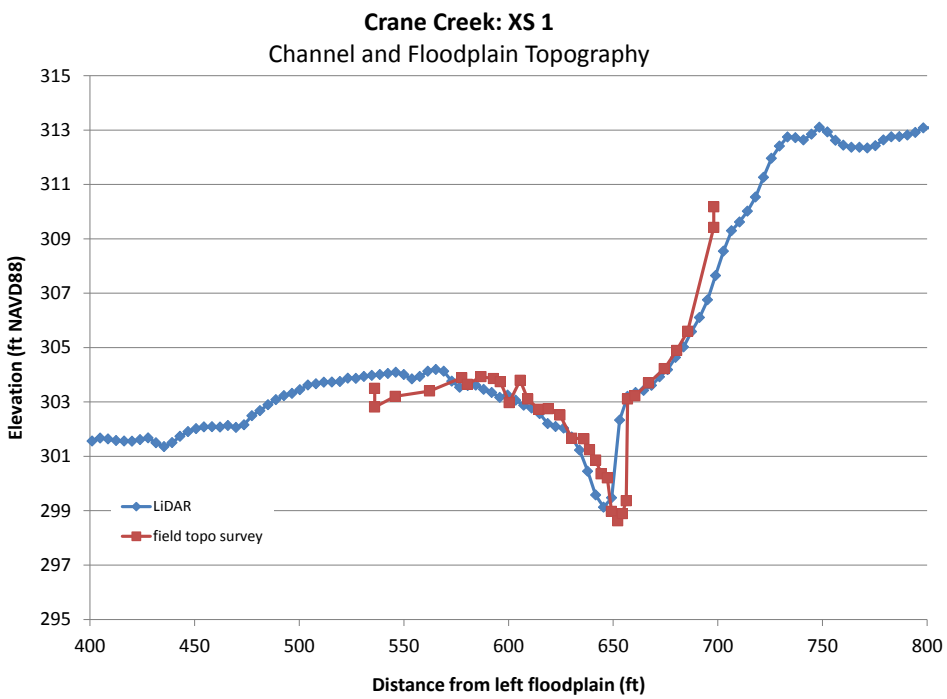

Figure B13. Crane Creek, cross-section 1 – LiDAR and field survey topography

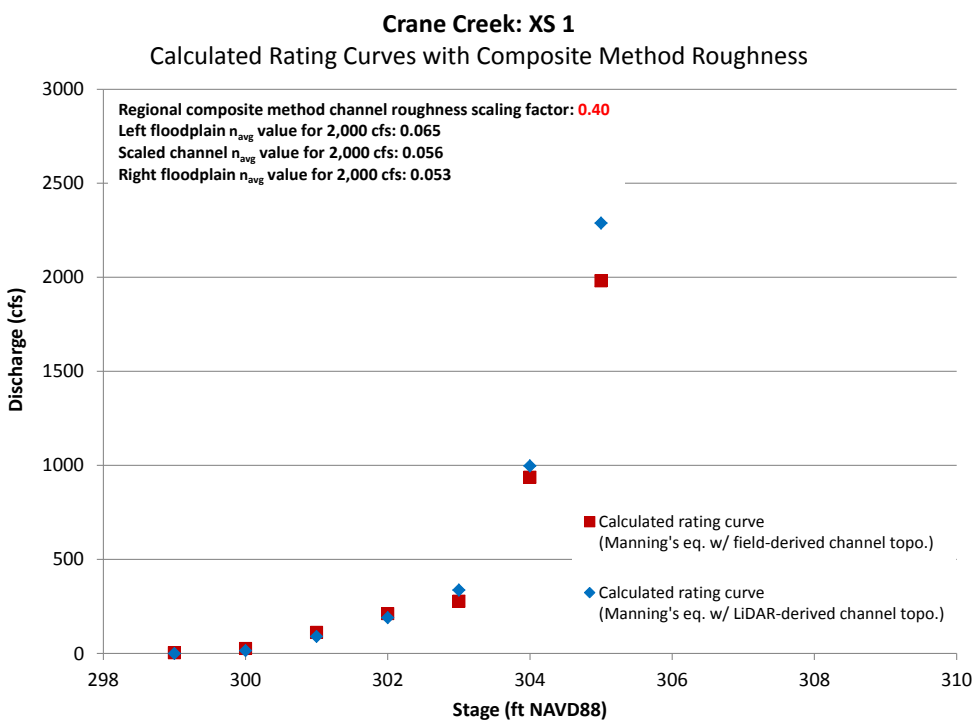

Figure B14. Crane Creek, cross-section 1 – calculated rating curves

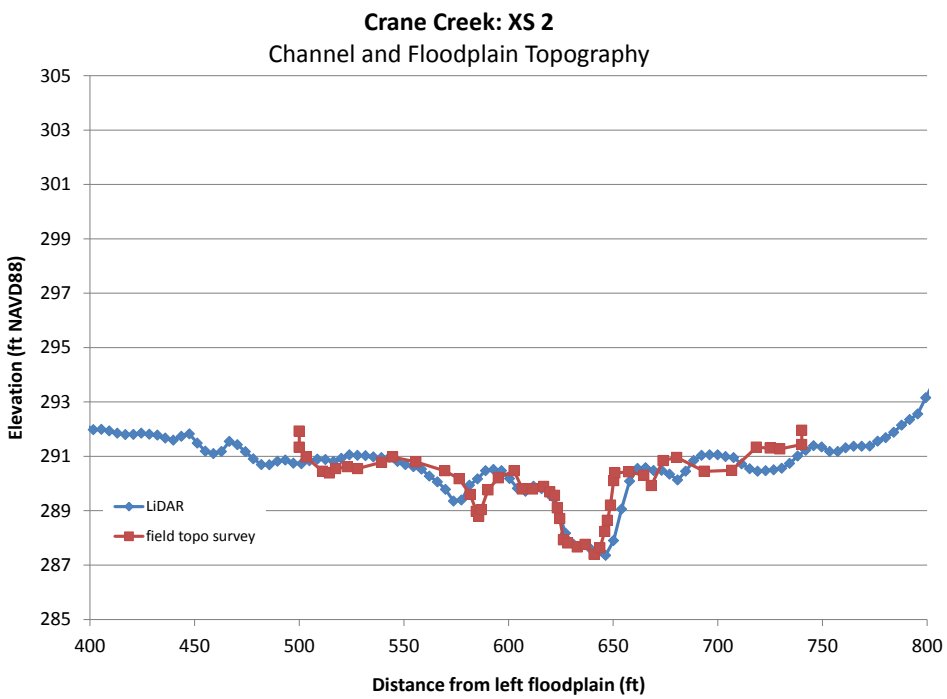

Figure B15. Crane Creek, cross-section 2 – LiDAR and field survey topography

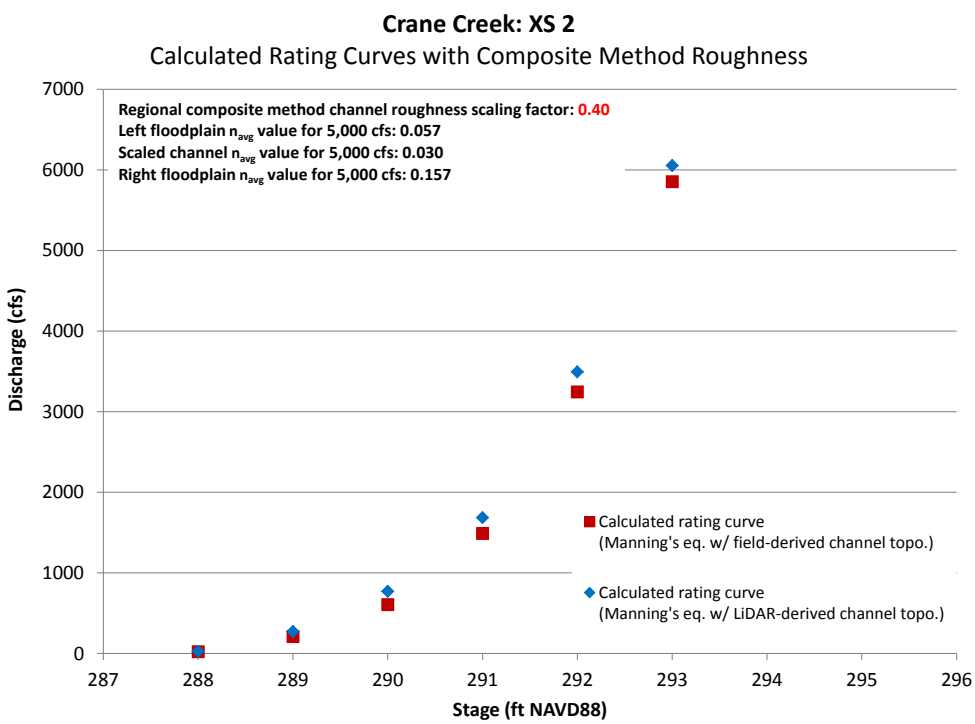

Figure B16. Crane Creek, cross-section 2 – calculated rating curves

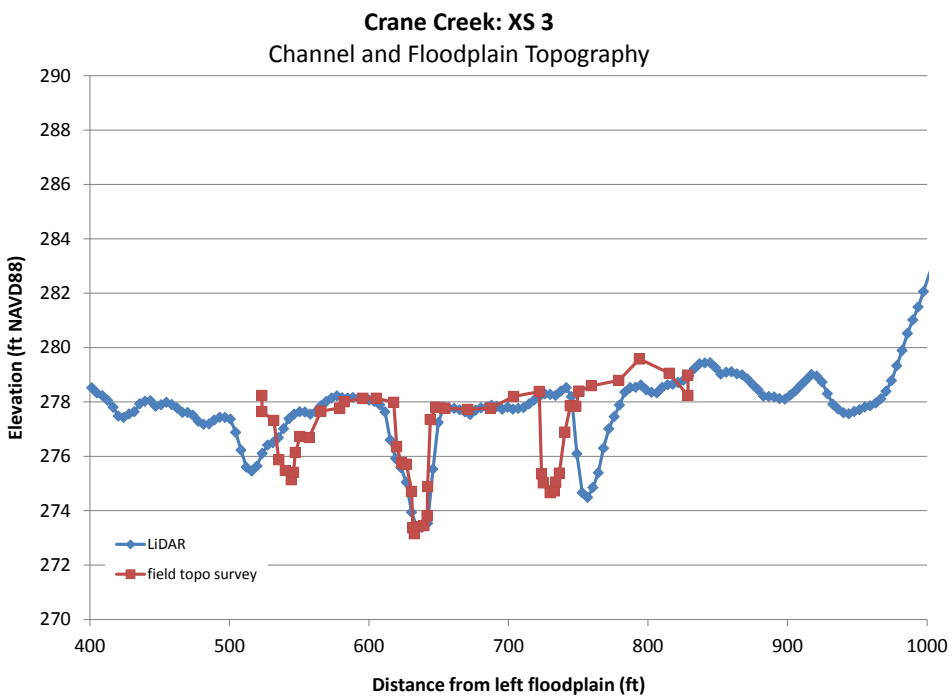

Figure B17. Crane Creek, cross-section 3 – LiDAR and field survey topography

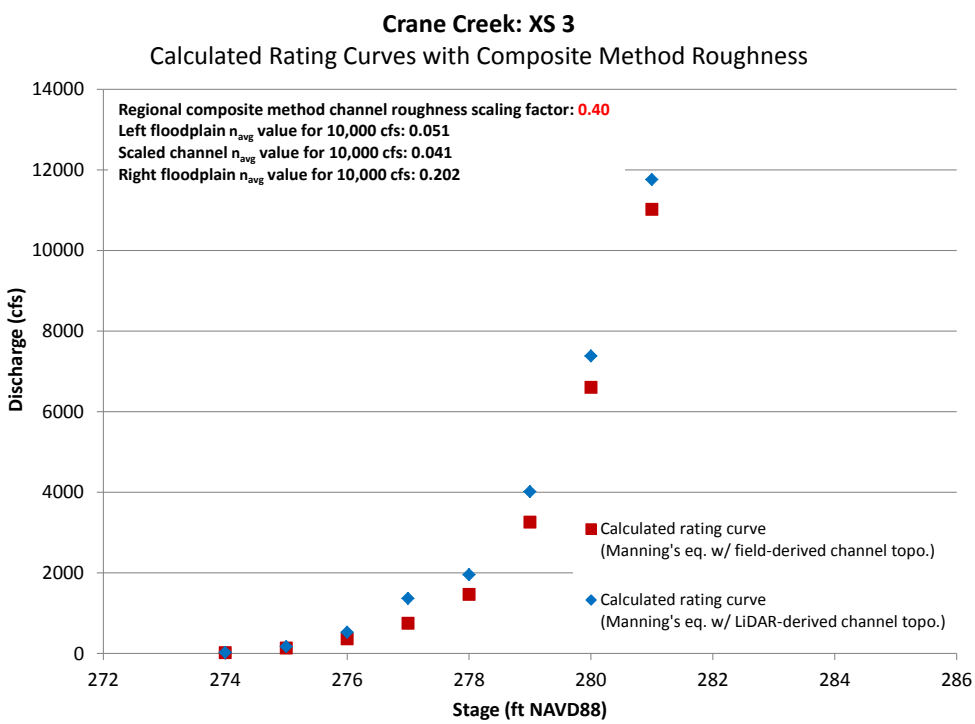

Figure B18. Crane Creek, cross-section 3 – calculated rating curves

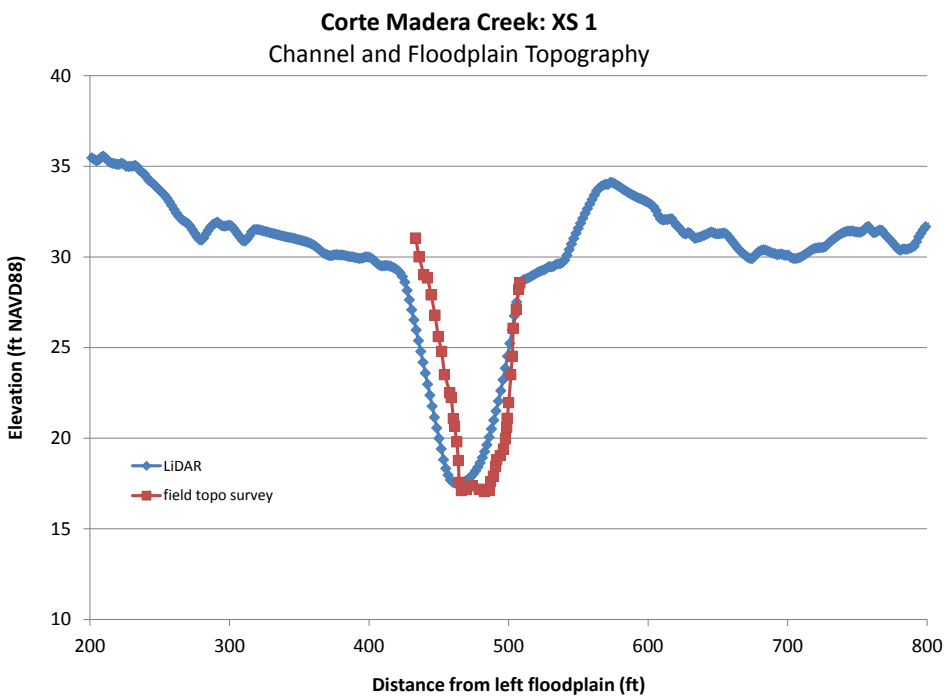

Figure B19. Corte Madera Creek, cross-section 1 – LiDAR and field survey topography

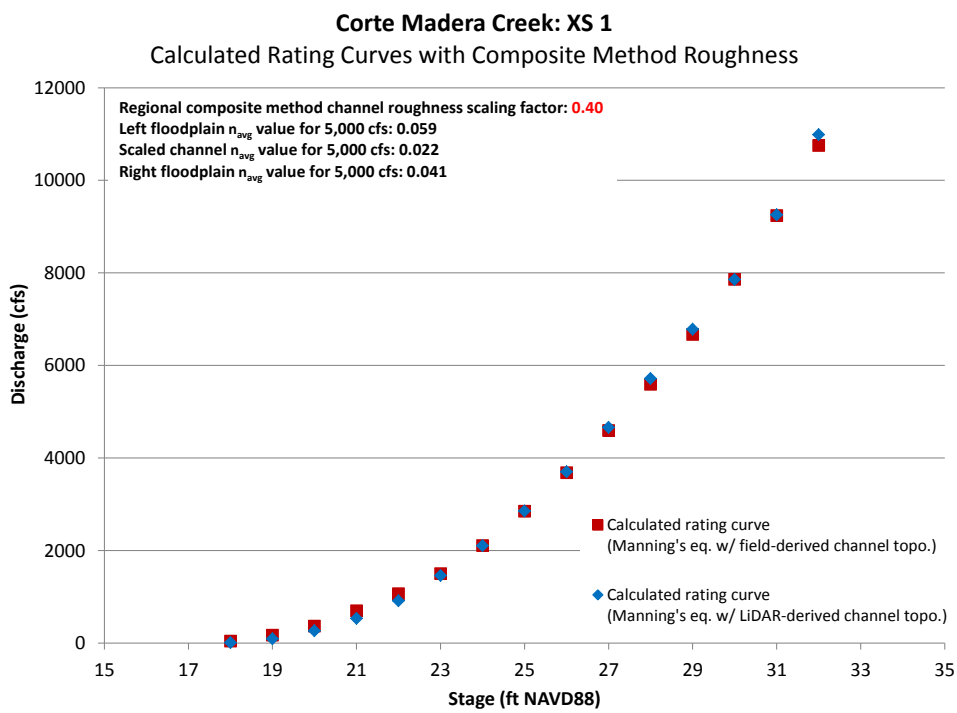

Figure B20. Corte Madera Creek, cross-section 1 – calculated rating curves

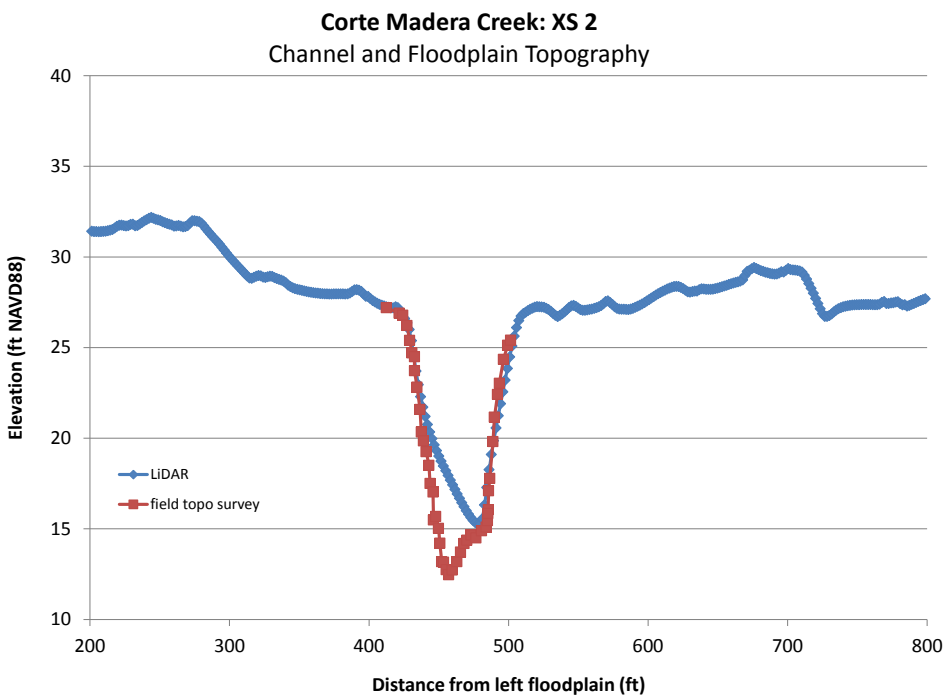

Figure B21. Corte Madera Creek, cross-section 2 – LiDAR and field survey topography

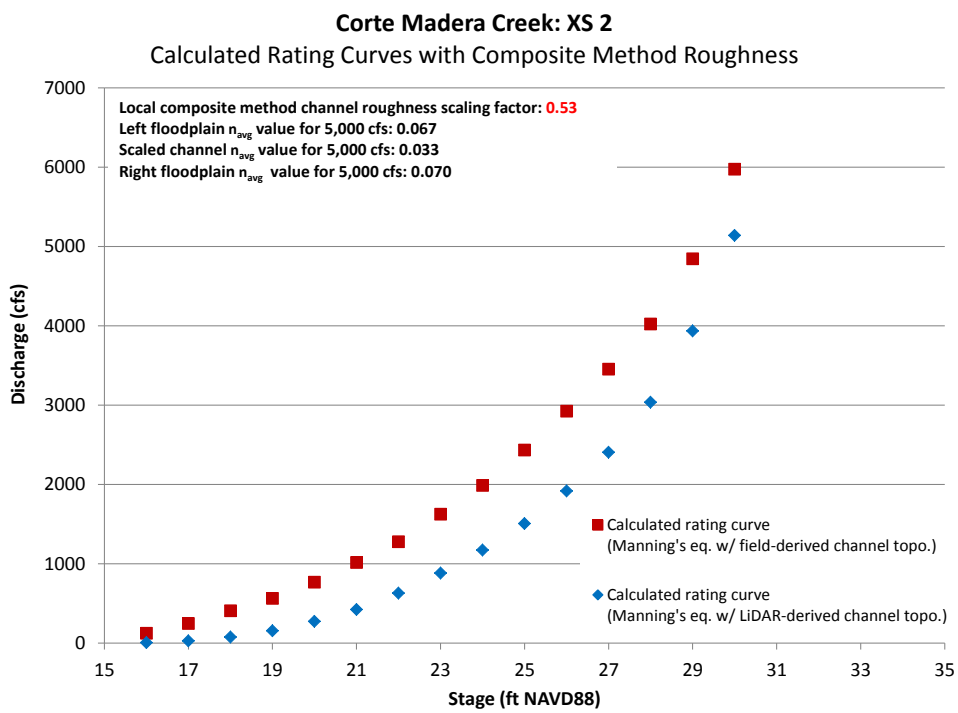

Figure B22. Corte Madera Creek, cross-section 2 – calculated rating curves

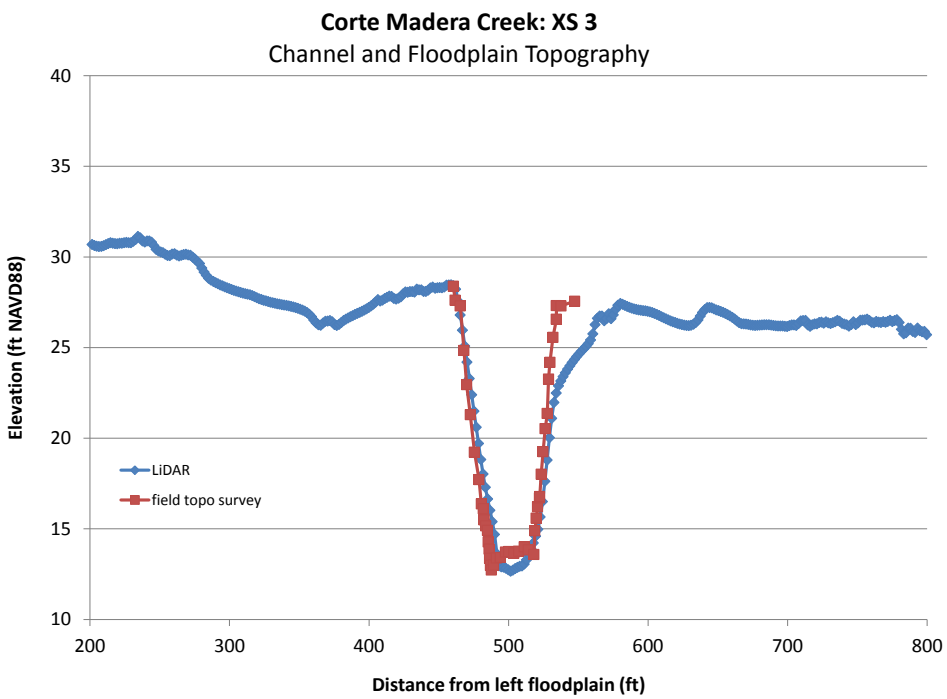

Figure B23. Corte Madera Creek, cross-section 3 – LiDAR and field survey topography

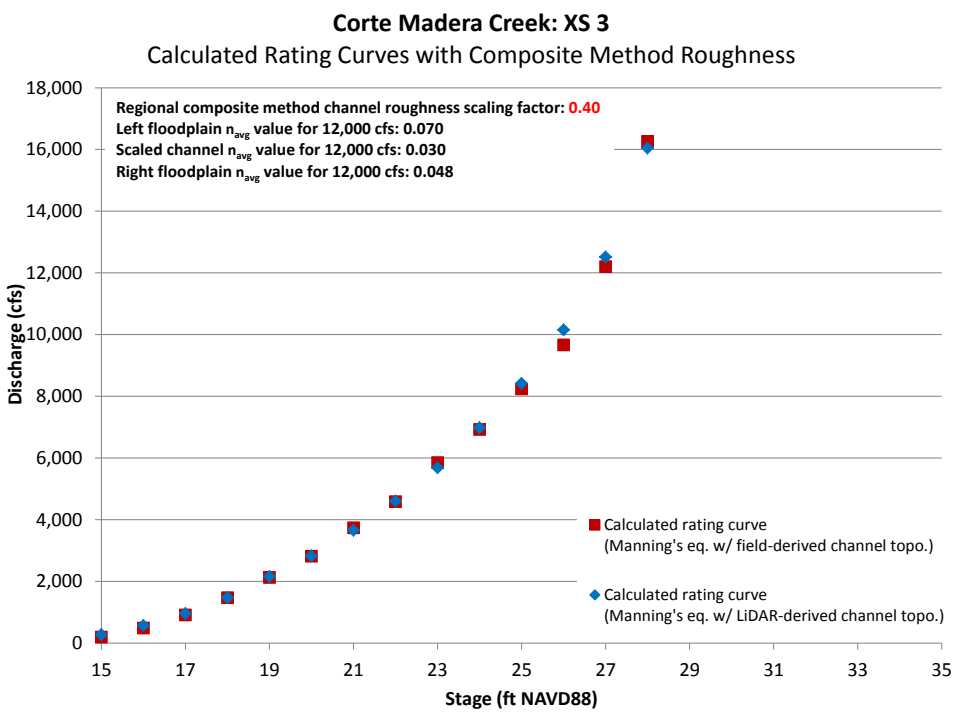

Figure B24. Corte Madera Creek, cross-section 3 – calculated rating curves

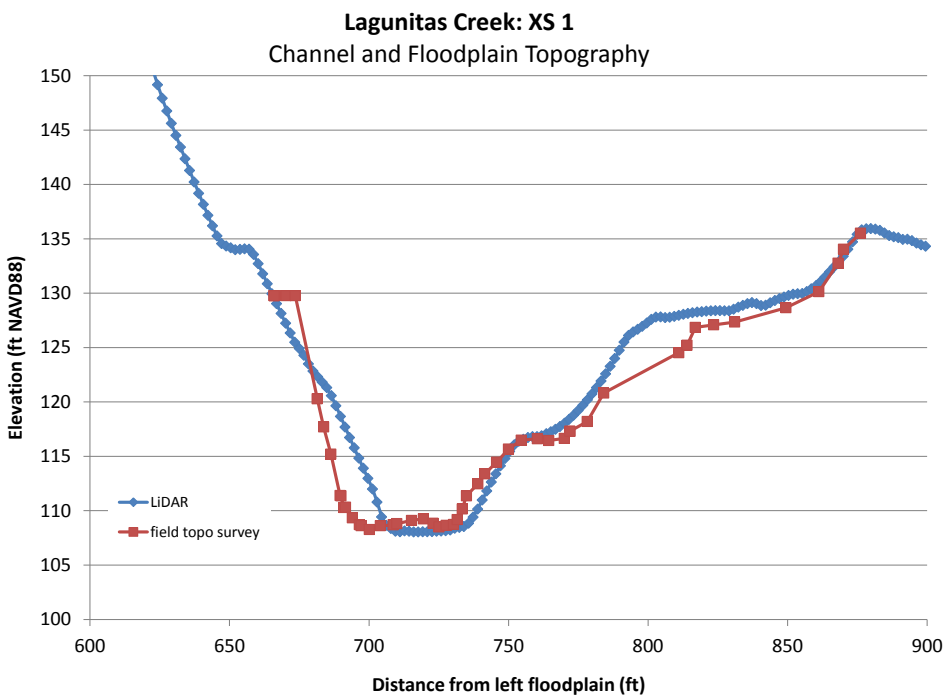

Figure B25. Lagunitas Creek, cross-section 1 – LiDAR and field survey topography

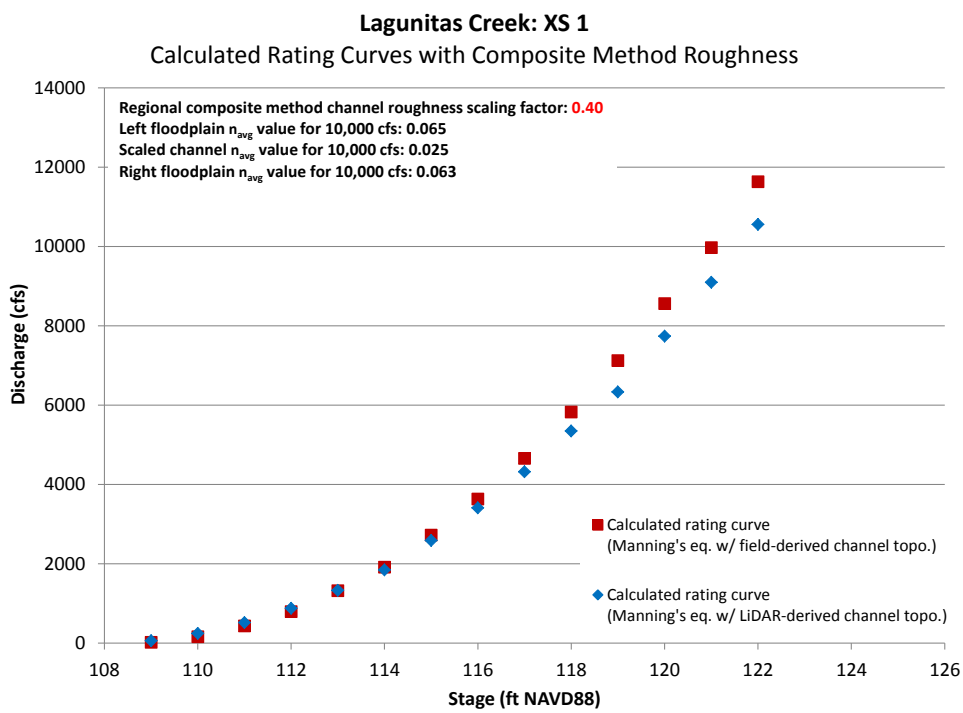

Figure B26. Lagunitas Creek, cross-section 1 – calculated rating curves

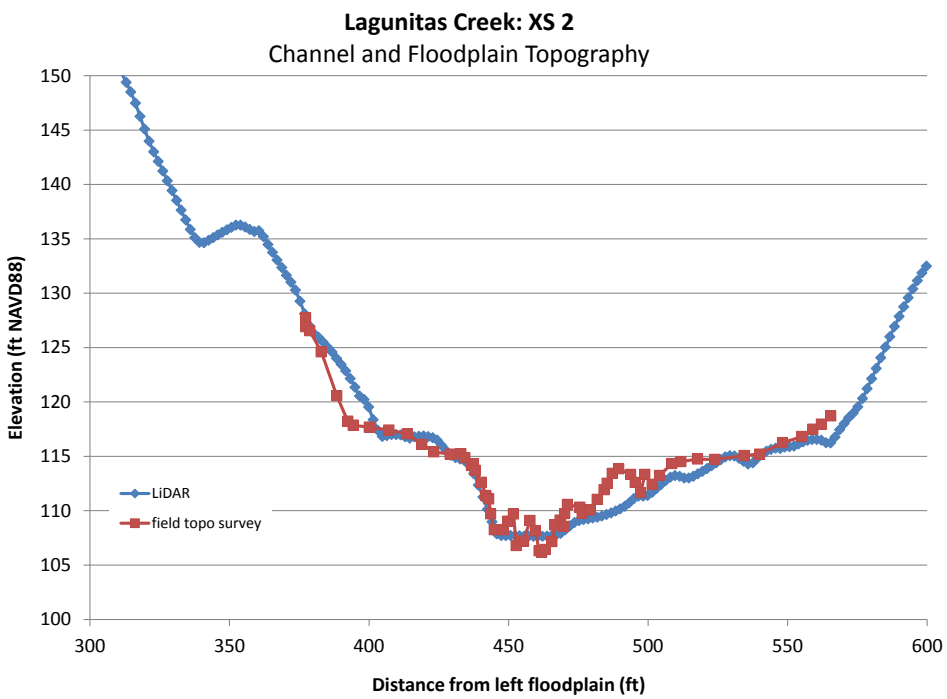

Figure B27. Lagunitas Creek, cross-section 2 – LiDAR and field survey topography

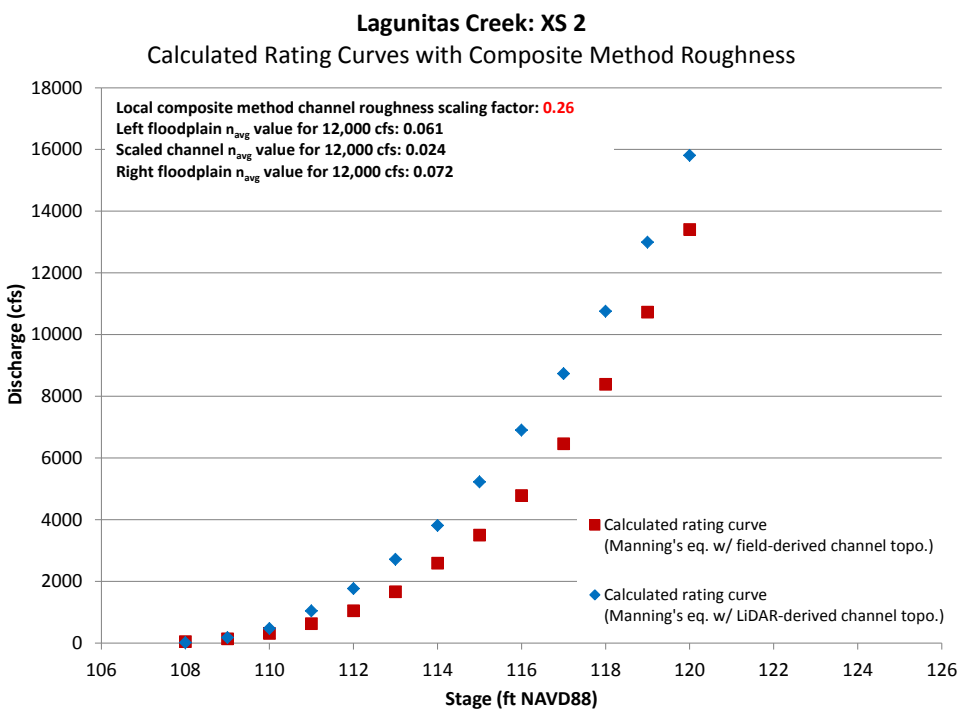

Figure B28. Lagunitas Creek, cross-section 2 – calculated rating curves

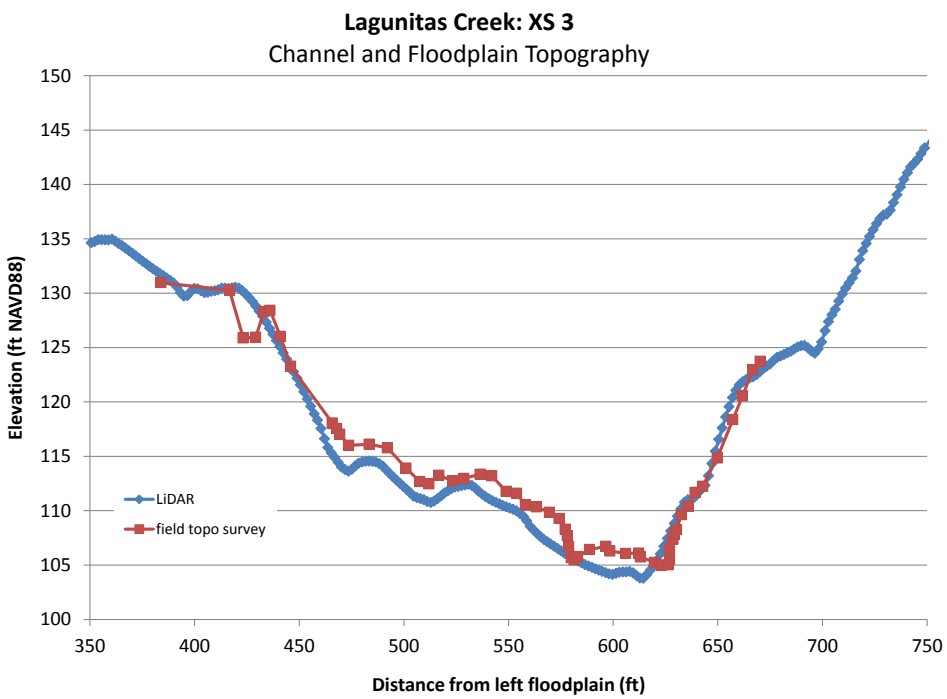

Figure B29. Lagunitas Creek, cross-section 3 – LiDAR and field survey topography

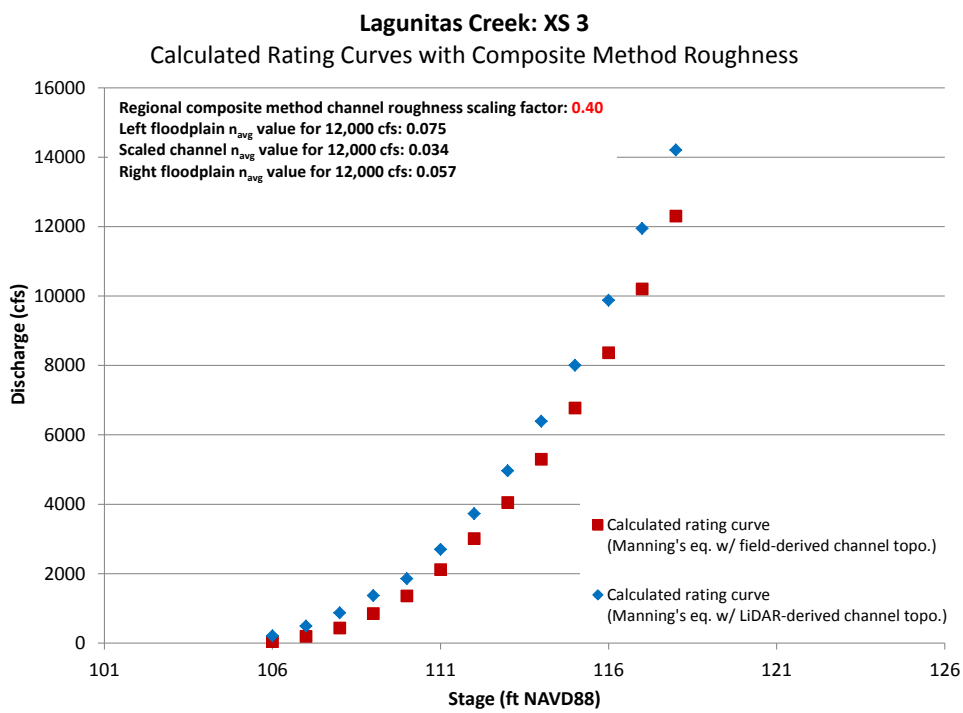

Figure B30. Lagunitas Creek, cross-section 3 – calculated rating curves

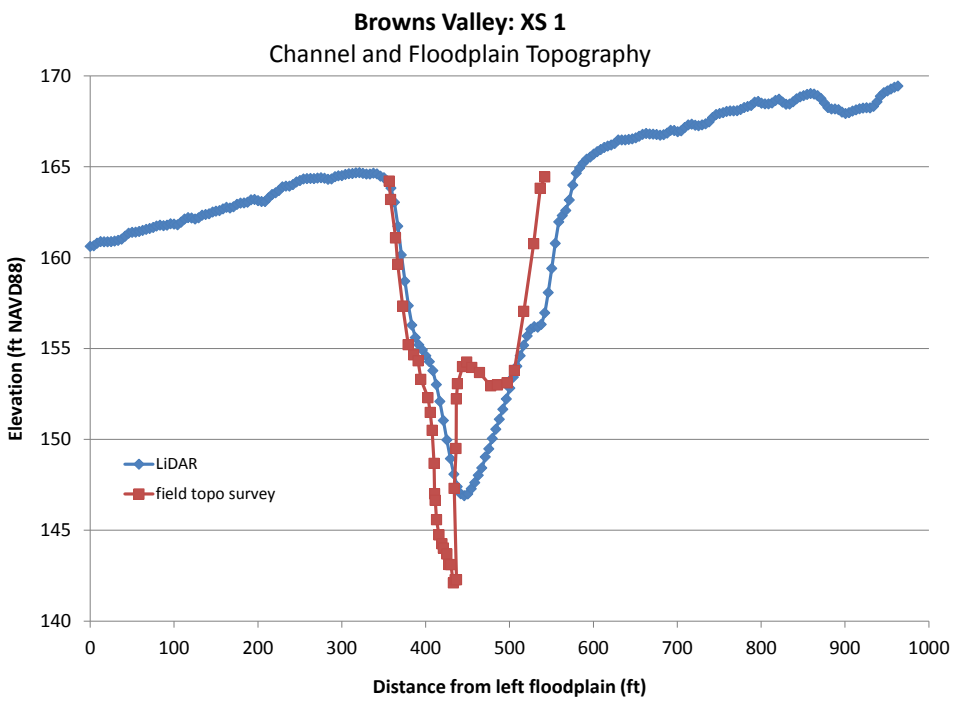

Figure B31. Browns Valley Creek, cross-section 1 – LiDAR and field survey topography

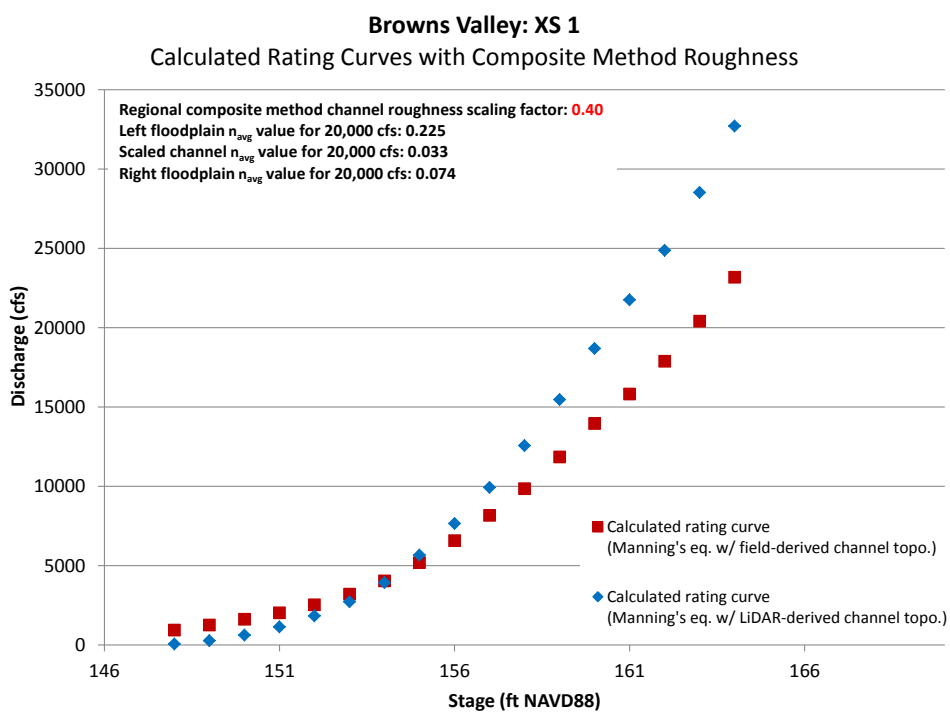

Figure B32. Browns Valley Creek, cross-section 1 – calculated rating curves

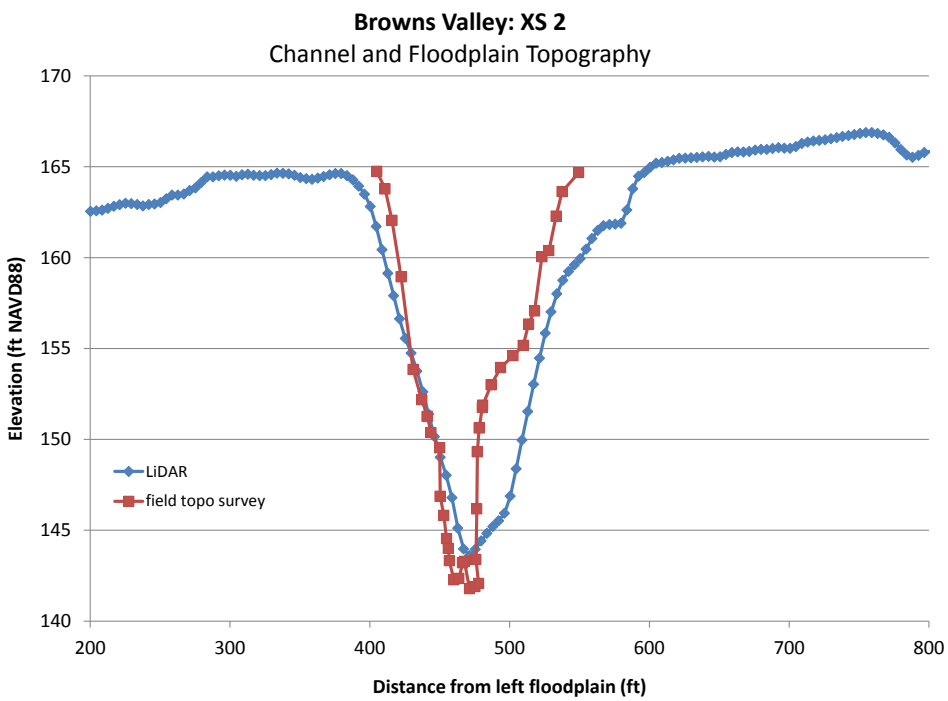

Figure B33. Browns Valley Creek, cross-section 2 – LiDAR and field survey topography

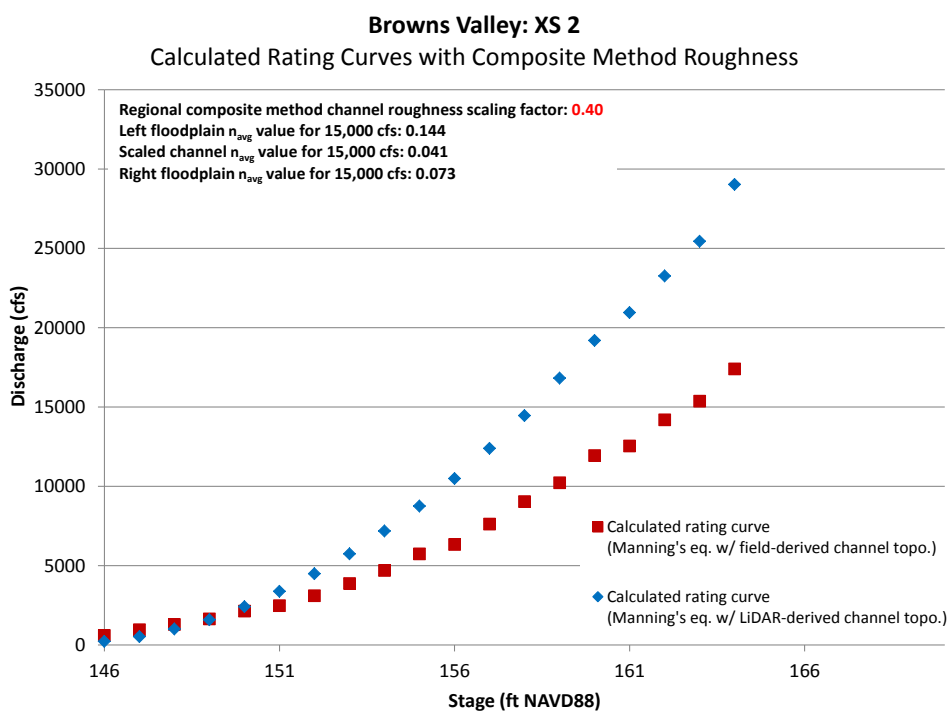

Figure B34. Browns Valley Creek, cross-section 2 – calculated rating curves

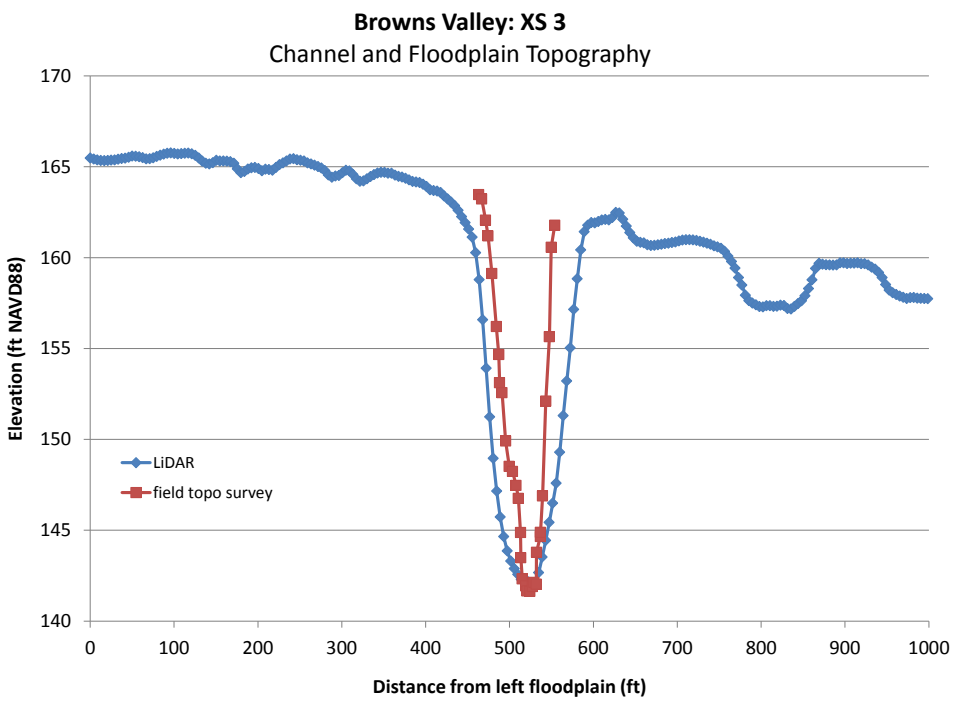

Figure B35. Browns Valley Creek, cross-section 3 – LiDAR and field survey topography

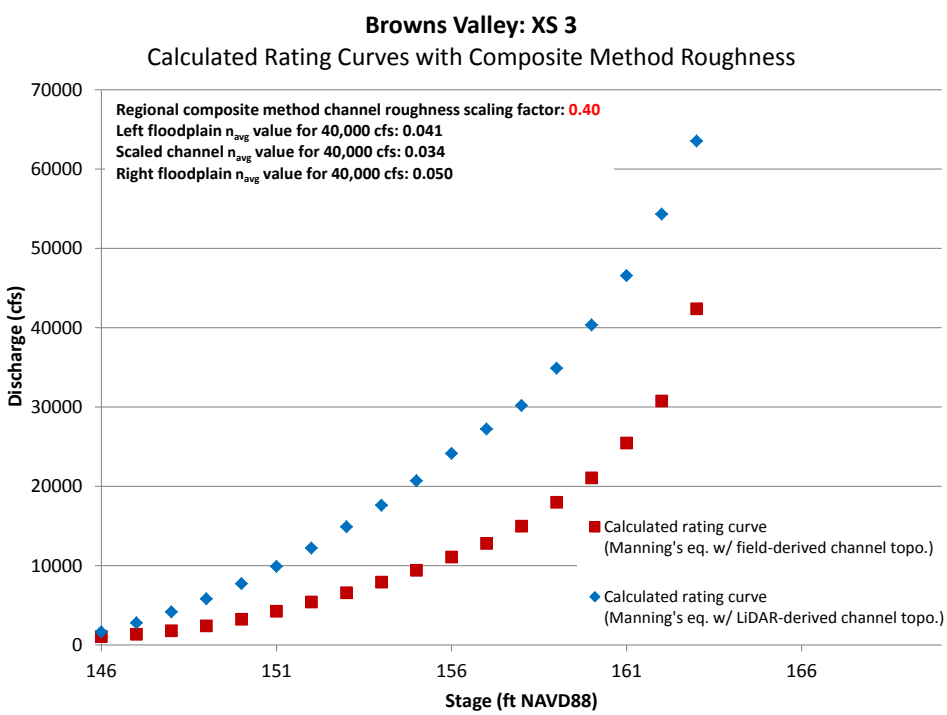

Figure B36. Browns Valley Creek, cross-section 3 – calculated rating curves

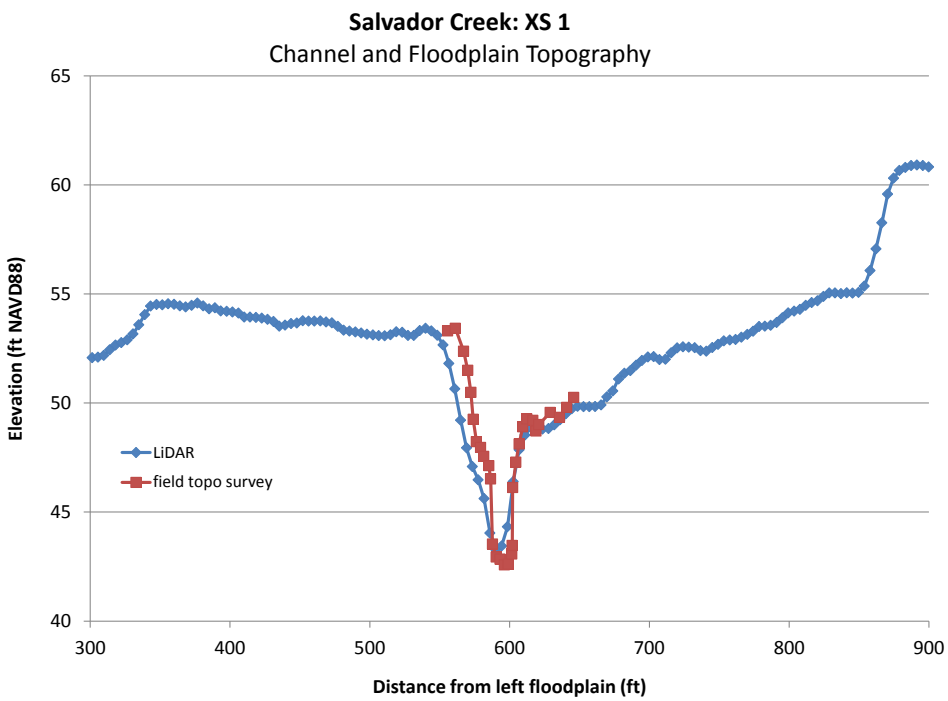

Figure B37. Salvador Creek, cross-section 1 – LiDAR and field survey topography

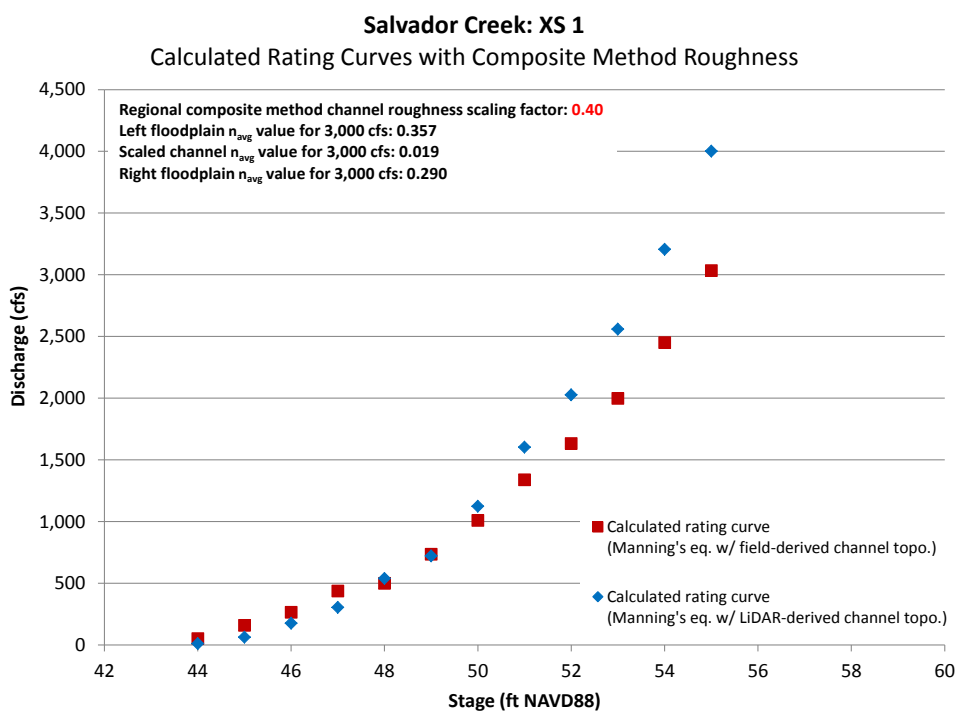

Figure B38. Salvador Creek, cross-section 1 – calculated rating curves

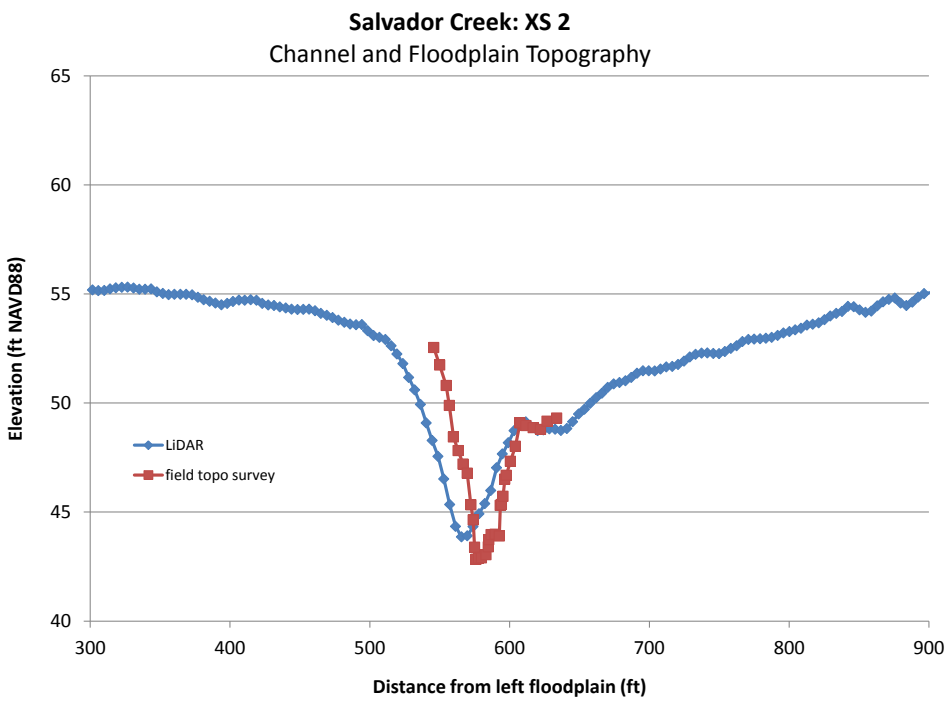

Figure B39. Salvador Creek, cross-section 2 – LiDAR and field survey topography

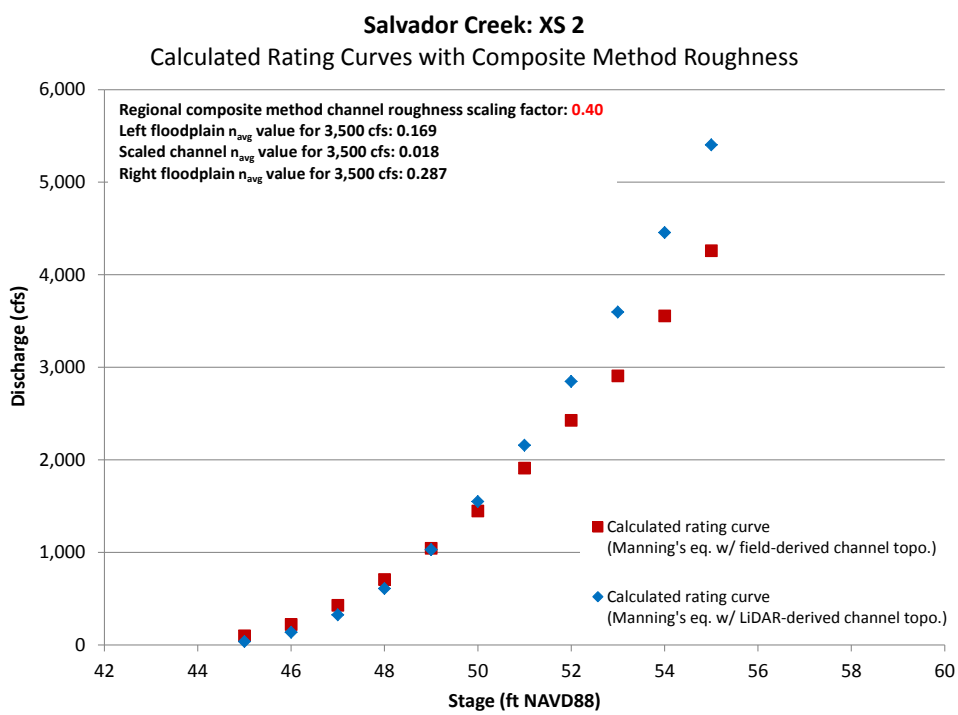

Figure B40. Salvador Creek, cross-section 2 – calculated rating curves

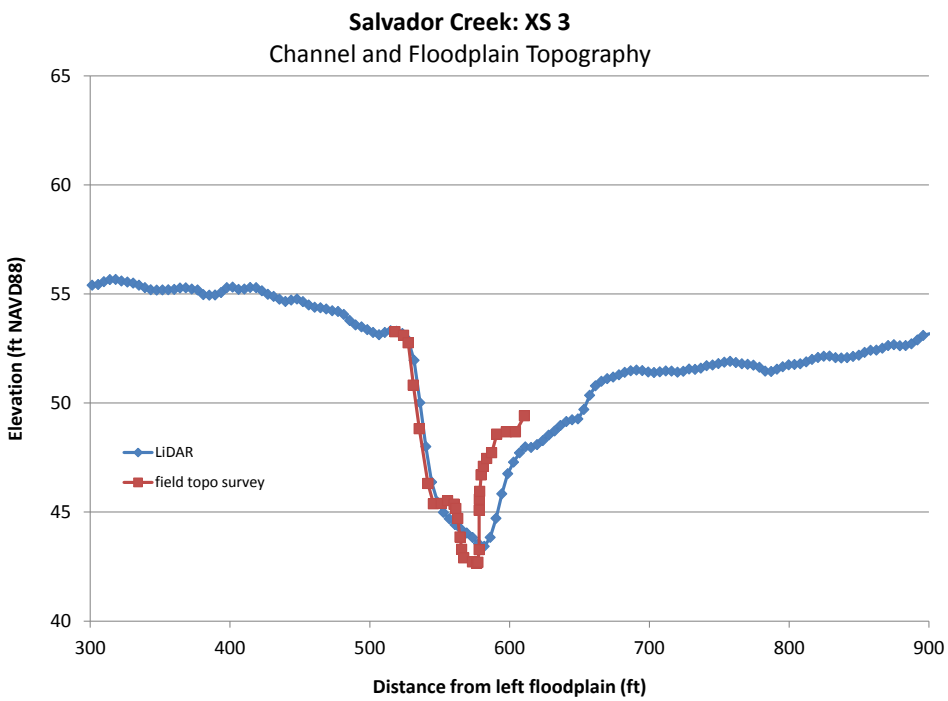

Figure B41. Salvador Creek, cross-section 3 – LiDAR and field survey topography

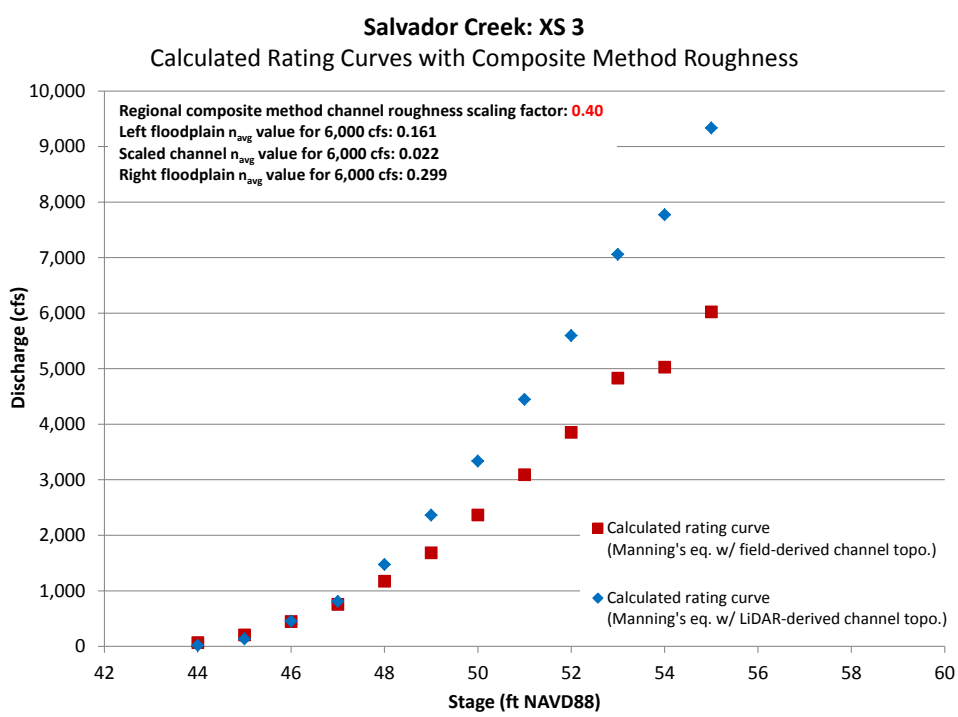

Figure B42. Salvador Creek, cross-section 3 – calculated rating curves

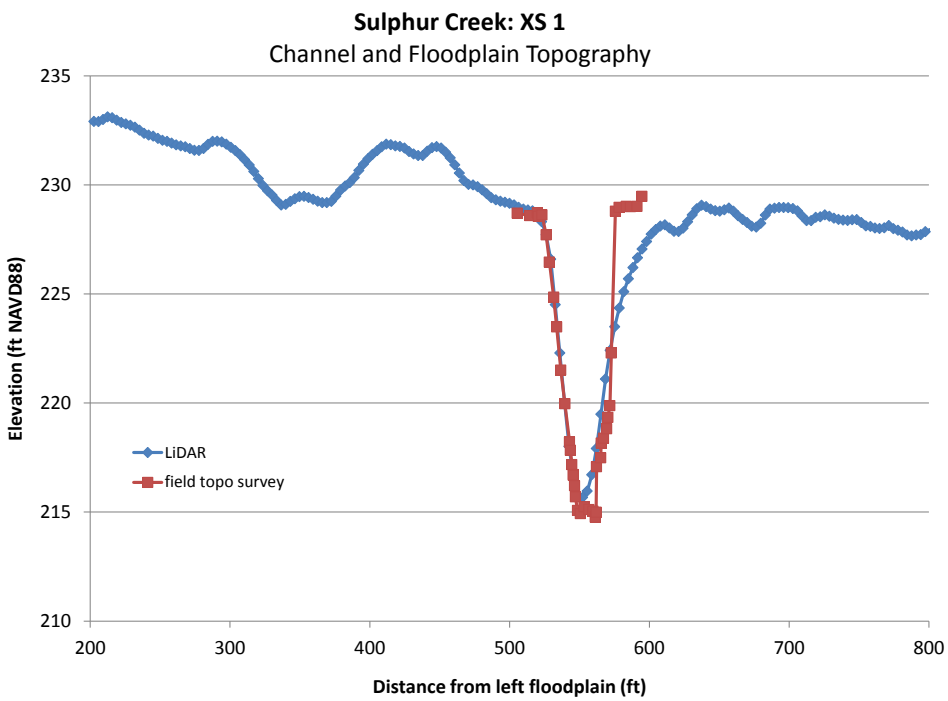

Figure B43. Sulphur Creek, cross-section 1 – LiDAR and field survey topography

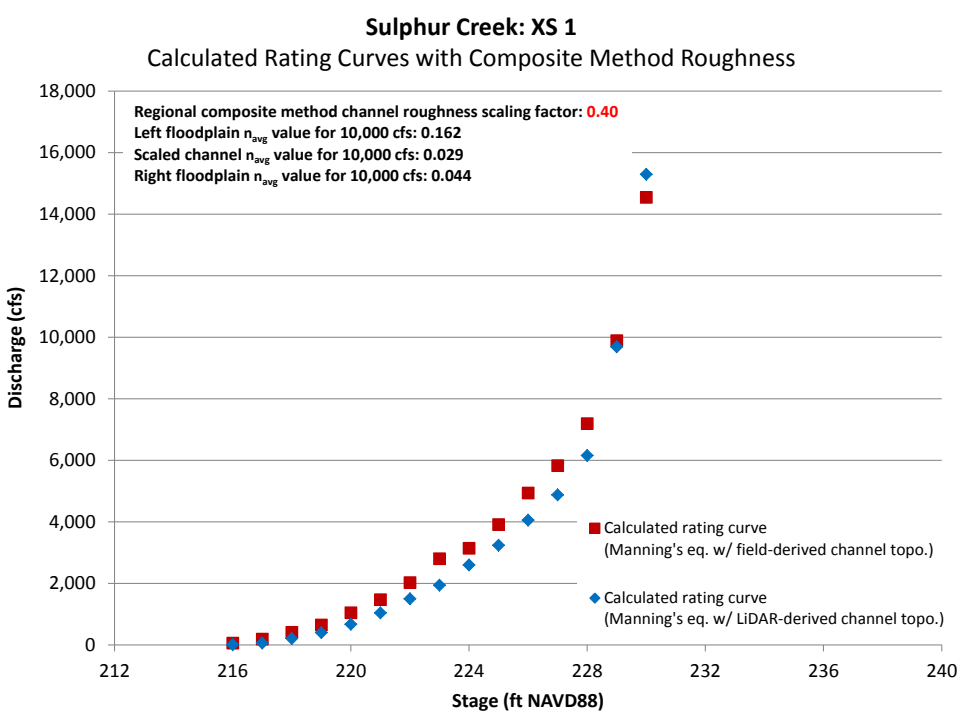

Figure B44. Sulphur Creek, cross-section 1 – calculated rating curves

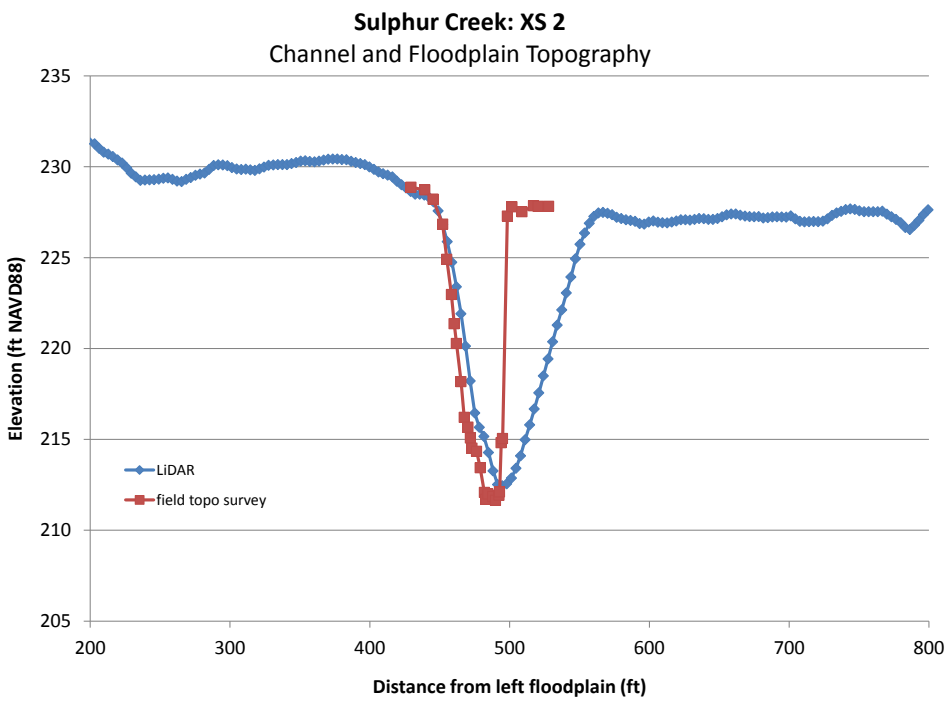

Figure B45. Sulphur Creek, cross-section 2 – LiDAR and field survey topography

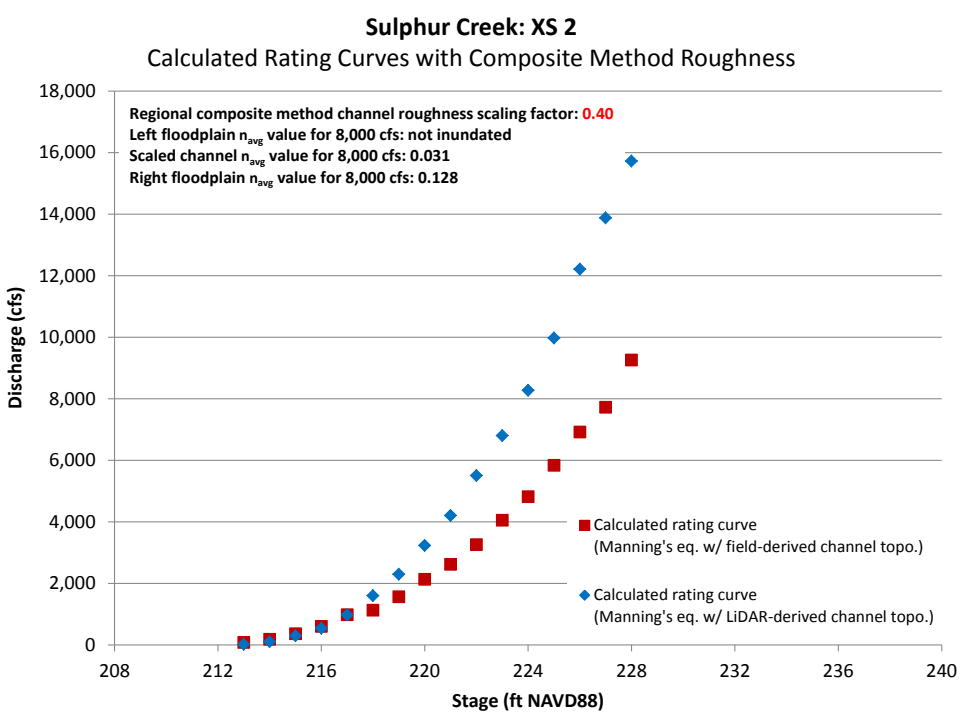

Figure B46. Sulphur Creek, cross-section 2 – calculated rating curves

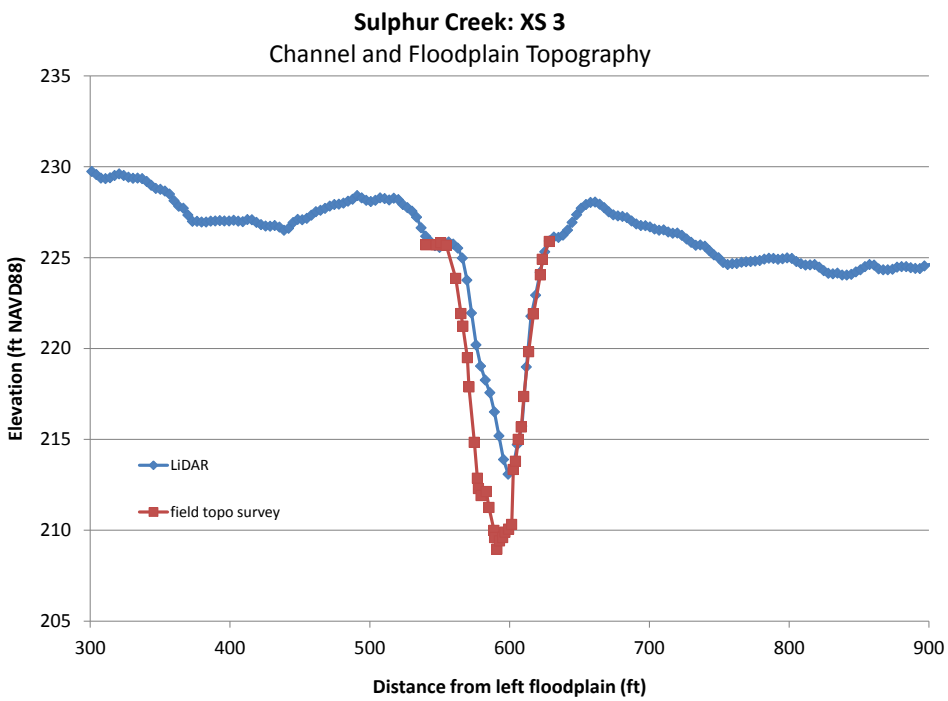

Figure B47. Sulphur Creek, cross-section 3 – LiDAR and field survey topography

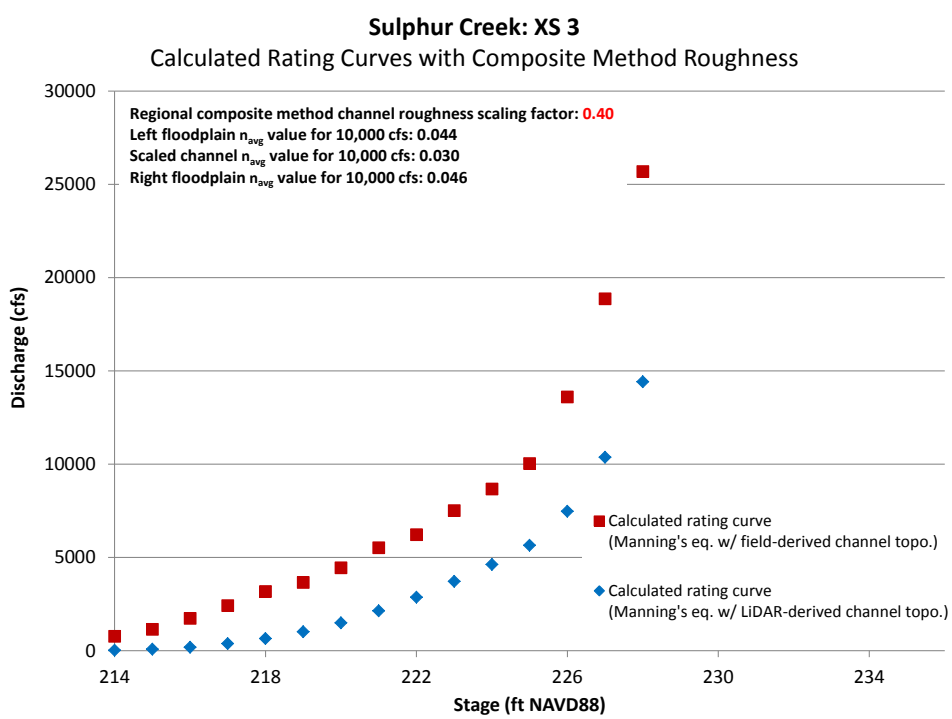

Figure B48. Sulphur Creek, cross-section 3 – calculated rating curves